Neurobiology of Disease 99 (2017) 66–83

Contents lists available at ScienceDirect

Neurobiology of Disease

journal homepage: www.elsevier.com/locate/ynbdi

The PRRT2 knockout mouse recapitulates the neurological diseases associated with *PRRT2* mutations

Caterina Michetti [a], Enrico Castroflorio [a,b], Ivan Marchionni [a], Nicola Forte [a], Bruno Sterlini [b], Francesca Binda [a], Floriana Fruscione [c], Pietro Baldelli [a,b], Flavia Valtorta [d], Federico Zara [c], Anna Corradi [a], Fabio Benfenati [a,b,*]

[a] Center for Synaptic Neuroscience and Technology, Istituto Italiano di Tecnologia, Largo Rosanna Benzi 10, 16132 Genova, Italy
[b] Department of Experimental Medicine, University of Genova, Viale Benedetto XV, 3, 16132 Genova, Italy
[c] Department Head and Neck Neuroscience, Laboratory of Neurogenetics and Neuroscience, Institute G. Gaslini, Via Gerolamo Gaslini, 5, 16148 Genova, Italy
[d] San Raffaele Scientific Institute and Vita Salute University, Via Olgettina 58, 20132 Milano, Italy

ARTICLE INFO

Article history:
Received 8 September 2016
Revised 6 December 2016
Accepted 18 December 2016
Available online 20 December 2016

Keywords:
Proline-rich transmembrane protein 2
Knockout mouse
Motor paroxysms
Audiogenic seizures
Synaptic transmission
Hippocampus
Cerebellum

ABSTRACT

Heterozygous and rare homozygous mutations in PRoline-Rich Transmembrane protein 2 (PRRT2) underlie a group of paroxysmal disorders including epilepsy, kinesigenic dyskinesia episodic ataxia and migraine. Most of the mutations lead to impaired PRRT2 expression and/or function. Recently, an important role for PRTT2 in the neurotransmitter release machinery, brain development and synapse formation has been uncovered. In this work, we have characterized the phenotype of a mouse in which the PRRT2 gene has been constitutively inactivated (PRRT2 KO). β-galactosidase staining allowed to map the regional expression of PRRT2 that was more intense in the cerebellum, hindbrain and spinal cord, while it was localized to restricted areas in the forebrain. PRRT2 KO mice are normal at birth, but display paroxysmal movements at the onset of locomotion that persist in the adulthood. In addition, adult PRRT2 KO mice present abnormal motor behaviors characterized by wild running and jumping in response to audiogenic stimuli that are ineffective in wild type mice and an increased sensitivity to the convulsive effects of pentylentetrazol. Patch-clamp electrophysiology in hippocampal and cerebellar slices revealed specific effects in the cerebellum, where PRRT2 is highly expressed, consisting in a higher excitatory strength at parallel fiber-Purkinje cell synapses during high frequency stimulation. The results show that the PRRT2 KO mouse reproduces the motor paroxysms present in the human PRRT2-linked pathology and can be proposed as an experimental model for the study of the pathogenesis of the disease as well as for testing personalized therapeutic approaches.

1. Introduction

Proline-rich transmembrane protein 2 (PRRT2)[1] is the causative gene for a variety of paroxysmal neurological disorders that can be grouped in three major phenotypes: Benign Familial Infantile Epilepsy (BFIE), Paroxysmal Kinesigenic Dyskinesia (PKD), and Infantile Convulsions with Choreoathetosis (ICCA)/Paroxysmal Kinesigenic Dyskinesia with Infantile Convulsions (PKD/IC) (Chen et al., 2011; Lee et al., 2012).

To date, some 1500 patients with 70 different PRRT2 mutations have been reported, 78% of which carrying the same frameshift mutation (c.649dupC). In addition to this frequent mutation, about 75% of all reported PRRT2 mutations involve the insertion of a precocious stop codon, leading to an unstable mRNA and/or a truncated protein that is degraded or mistargeted (Chen et al., 2011; Lee et al., 2012; Li et al., 2015; Liu et al., 2016; Valtorta et al., 2016). Of the 22 reported missense mutations, 16 were not found or were found only once in >60,000 exomes, indicating the high likelihood of their pathogenicity.

The core of PRRT2-associated disorders consists of three diseases BFIE, PKD and PKD/IC forming a continuous spectrum. PRRT2 mutations account for the majority of familial BFIE, PKD and PKD/IC patients and, conversely, 95% of PRRT2 patients have a diagnosis within the BFIE–PKD/IC–PKD spectrum. In addition, a low percentage (5%) of patients bearing PRRT2 mutations display other disorders such as episodic

* Corresponding author at: Center for Synaptic Neuroscience and Technology, Fondazione Istituto Italiano di Tecnologia, Via Morego 30, 16163 Genoa, Italy.
E-mail address: fabio.benfenati@iit.it (F. Benfenati).

Available online on ScienceDirect (www.sciencedirect.com).

[1] AGS, audiogenic seizures; ACSF, artificial cerebrospinal fluid; BFIE = Benign Familial Infantile Epilepsy; β-gal, β-galactosidase; CNS, central nervous system; CS, conditioned stimulus; DG, dentate gyrus; EEG, electroencephalogram; eEPSC, evoked excitatory postsynaptic current; eIPSC, evoked inhibitory postsynaptic current; GC, granule cell; HET, heterozygous knockout; ICCA, Infantile Convulsions with Choreoathetosis; ISI, inter-stimulus interval; KO, homozygous knockout; mEPSC, miniature excitatory postsynaptic current; mIPSC, miniature inhibitory postsynaptic current; NGS, normal goat serum; P, postnatal day; PB, phosphate buffer; PBS, phosphate buffered saline; PC, Purkinje cell; PF, parallel fiber; PKD, Paroxysmal Kinesigenic Dyskinesia; PKD/IC, Paroxysmal Kinesigenic Dyskinesia with Infantile Convulsions; PPR, paired-pulse ratio; PTZ, pentylentetrazol; PRRT2, proline-rich transmembrane protein 2; TTX, tetrodotoxin; US, unconditioned stimulus; WT, wild type

http://dx.doi.org/10.1016/j.nbd.2016.12.018

ataxia, hemiplegic migraine, developmental delay and intellectual disability. The noticeable pleiotropy of the phenotypes associated with PRRT2 mutations is not reflected by specific genotype-phenotype correlations (Ebrahimi-Fakhari et al., 2015; Gardiner et al., 2015; Heron and Dibbens, 2013; Valtorta et al., 2016).

In BFIE, patients exhibit afebrile seizures starting from 6 months to about 2 years of age and including clusters of focal or generalized attacks with normal interictal EEG and MRI (Scheffer et al., 2012; Vigevano, 2005). PKD-affected patients are characterized by short and frequent episodes of dystonic or choreiform movements triggered by sudden voluntary movements or startle with onset in childhood or adolescence (Ebrahimi-Fakhari et al., 2015). In the ICCA syndrome, patients exhibit infantile seizures, movement disorders or both. All the above-described syndromes are characterized by paroxysmal attacks that occur periodically, suggesting the existence of common underlying pathophysiological mechanisms (Valtorta et al., 2016). The few patients bearing homozygous or compound heterozygous mutations in *PRRT2* show a severe encephalopathic phenotype, with paroxysmal dyskinesias, unusually prolonged ataxia attacks, seizures and intellectual disability (Delcourt et al., 2015; Huang et al., 2015; Labate et al., 2012). However, until very recently, knowledge concerning the molecular mechanisms by which PRRT2 mutations cause the disease and manifest with different phenotypes remained scarce. The association of PRRT2-linked pathologies with haploinsufficiency, as well as the more severe phenotype of homozygous mutations, indicate that the disorders are attributable to loss-of-function of the protein and gene-dosage effects and suggest that the silencing or the constitutive deletion of the PRRT2 gene in the mouse can be a valid model to study the pathogenesis of the PRRT2-linked diseases.

A series of very recent papers have shown that PRRT2 is involved in brain development, synapse formation and neurotransmitter release (Liu et al., 2016; Valente et al., 2016). PRRT2 is a type II transmembrane protein with a C-terminal anchor, resembling the SNARE proteins VAMP/synaptobrevin and syntaxin (Rossi et al., 2016). In humans and rodents, PRRT2 is neuron-specific and is expressed with the highest levels in cerebellum, basal ganglia and neocortex. In the cortex and hippocampus, PRRT2 is already expressed at early postnatal stages, a postnatal stages, and its expression increases to reach a plateau at 1 month of life over a period of synapse formation and rearrangement (Chen et al., 2011; Ebrahimi-Fakhari et al., 2015; Valente et al., 2016). In neurons, PRRT2 has a distal distribution with the highest levels at synapses, where it mostly codistributes with proteins associated with the presynaptic area and, to a much lower extent, in fractions enriched in post-synaptic densities (Lee et al., 2012; Liu et al., 2016; Valente et al., 2016).

Acute silencing of PRRT2 by RNA interference during *in vitro* development was shown to cause a decrease in the density of synaptic connections (Valente et al., 2016) that was paralleled *in vivo* by a delayed radial migration of neurons and a decreased density of synaptic spines (Liu et al., 2016). Interestingly, PRRT2 silencing in primary neurons was followed by a severe impairment in synchronous release, while the asynchronous release was relatively preserved (Valente et al., 2016). This cellular phenotype was supported by the observation that, at the presynaptic level, PRRT2 interacts with the fast Ca^{2+} sensors synaptotagmins 1 and 2 and with SNAP25 and VAMP/synaptobrevin, endowing the SNARE complex with Ca^{2+} sensitivity for fast synchronous neurotransmitter release (Boyken et al., 2013; Lee et al., 2012; Valente et al., 2016).

Here, we have for the first time characterized a genetically altered mouse constitutively lacking PRRT2 that also allowed us to analyze PRRT2 expression by means of a knocked-in lacZ sequence. We find that PRRT2 is abundantly expressed in the hindbrain neurons and in restricted populations of forebrain neurons. PRRT2 knockout (KO) mice display a pleiotropic paroxysmal phenotype during infancy and in the adulthood with paroxysmal dyskinesias in response to audiogenic stimuli and an increased sensitivity to the convulsive effects of pentylentetrazol (PTZ). Thus, the PRRT2 KO mouse reproduces multiple aspects of the human pathology associated with PRRT2 mutations and can therefore be used as a reliable experimental model of PRRT2-linked neurological disorders.

2. Materials and methods

2.1. Experimental animals and housing

Heterozygous PRRT2 KO mice were kindly provided by the IMPC European Consortium at the Sanger Institute (UK) in the frame of the European EMMA/Infrafrontier, and bred at the IIT SPF animal facility. The EUCOMM/KOMP targeting strategy was based on the "knockout-first" allele that contains an IRES:lacZ trapping cassette and a floxed neo cassette that were inserted into the intronic region among the exons 1 and 2 of the PRRT2 wild type locus (Fig. S1A). The presence of an Engrailed (En2) splice acceptor disrupts gene function, resulting in a lacZ fusion for studying gene expression localization (Skarnes et al., 2011). Genotyping was performed by PCR with primers Prrt2_F: AGGTAGACGGGCATTTGAGC, Prrt2_R: CGTGGGGAAGAGGAGACAAC; CAS_R1_Term: TCGTGGTATCGTTATGCGCC, that were used to detect the wild-type (WT) (Prrt2_F plus Prrt2_R product, 480 bp) and mutant (Prrt2_F plus CAS_R1_Term product, 200 bp) PRRT2 alleles and to genotype WT, heterozygous (HET) and KO mice. The primer Prrt2 F is common to wild type and mutant PCR and was designed in the intronic sequence between Prrt2 Exon 1 and Exon 2. The primer Prrt2 R was designed in the exon 2 of PRRT2 gene and the Cas_R1_Term was designed in the targeting cassette (Fig. S1A). The colony was maintained on a C57BL/6N background and propagated in heterozygosity. Two females were housed with one male in standard Plexiglas cages (33 × 13 cm), with sawdust bedding and a metal top. After two weeks of mating, male mice were removed and dams were housed individually in Plexiglas cages and daily checked for delivery. Mice were maintained on a 12∶12 h light/dark cycle (lights on at 7 a.m.). The temperature was maintained at 21 ± 1 °C, relative humidity (60 ± 10%). Animals were provided drinking water and a complete pellet diet (Mucedola, Settimo Milanese, Italy) *ad libitum*. Mouse genotypes were determined at weaning (at P25) by RT-PCR on tail samples. Mice were weaned into cages of same sex pairs. All experiments were carried out in accordance with the guidelines established by the European Communities Council (Directive 2010/63/EU of March 4th, 2014) and were approved by the Italian Ministry of Health (authorization n. 73/2014-PR and n. 1276/2015-PR).

2.2. X-gal (β-galactosidase) staining

Brains isolated from HET and PRRT2 KO mice at various postnatal day (P) stages (P4, P8 and P16 up to 2 months of age) were fixed with 2% paraformaldehyde/0.2% glutaraldehyde solution, permeabilized in wash buffer (1% sodium deoxycolate, 2% NP-40, $MgCl_2$ 0.1 M), included in 2.5% agarose and cut with a microtome (Bioptica). Coronal sections (120 μm) were incubated with X-Gal solution (X-Gal 100 mg/ml, ferrocyanide potassium 2 mg/ml, ferricyanide potassium 1.64 mg/ml in Wash Buffer) for 6 h (P4, P8 mice) and overnight (P16, P60 mice) at 37 °C as previously described (Gazzerro et al., 2012). The entire slices were acquired at 20× while higher magnifications were acquired at 40×. Sections were analyzed with Neurolucida software (MicroBrightField) connected to a Nikon E-800 microscope *via* a color CCD camera. The identification of the specific β-gal-positive areas was performed using the Paxinos mouse brain atlas (Paxinos and Franklin, 2012) and the interactive Allen Brain Explorer atlas (The Allen Institute, http://mouse.brain-map.org/static/brainexplorer).

2.3. Western blotting

Protein concentration of the samples was determined using the BCA assay and equivalent amounts of protein were subjected to SDS-PAGE

on 10–12% polyacrylamide gels and blotted onto nitrocellulose membranes (Whatman). Blotted membranes were blocked for 1 h in 5% milk in Tris-buffered saline (10 mM Tris, 150 mM NaCl, pH 8.0) plus 0.1% Tween-20 and incubated overnight at 4 °C with anti-PRRT2 (1:500, Sigma-Aldrich) and anti-calnexin (1:5000, Sigma-Aldrich) polyclonal primary antibodies. Membranes were washed and incubated for 1 h at room temperature with peroxidase-conjugated goat anti-rabbit (1:5000; Bio-Rad) antibodies and immunoreactive protein bands were revealed with the ECL chemiluminescence detection system (Thermo Scientific, Waltham, Ma, USA).

2.4. Real time PCR

Total RNA was isolated from different brain areas using QIAzol Reagent (QIAGEN, Ilden, D) according to the manufacturer's instructions. The RNA yield and A260/280 ratio were quantified by using the Nanodrop-1000 spectrophotometer (Thermo Fisher Scientific, Waltham, USA). Subsequently, the samples were treated with RNase-free DNase to remove possible traces of genomic DNA. cDNA synthesis was then performed on 2 μg of total RNA using the GoScript reverse transcription system (Promega, Madison, USA) and random primers, following manufacturer's instructions and including RT- negative controls. Real time PCR analyses were performed using the SYBR Green I Master mix (Roche), on a CFX96 Touch Real-Time PCR Detection System (Biorad), with the following protocol: 95 °C for 10 min; 30 s at 95 °C/20 s at the specific annealing temperature (Ta)/30 s at 72 °C for 45 cycles; melting curve (heating ramp from 55 °C to 95 °C) in order to check for amplification specificity. The following primers (final concentration 0.25 μM) and annealing temperatures were used:

PRRT2 For: CCACAATGTTGACAGGCCAC, Ta = 59.69 °C;
PRRT2 Rev: GAAGGCACCCAGAAACCTCG, Ta = 60 °C;
SNAP25 For: GCATTGAAGAAGAAACCTCGGG, Ta = 59.84 °C;
SNAP25 Rev: GGTAGCAAGAGTGGAGGAGC, Ta = 59.82 °C;
VGAT For: TGTCCTATCCGTTGCCCTTC, Ta = 59.46 °C;
VGAT Rev: CATAGCAGGCGGGGAAGAAG, Ta = 60.53 °C;
VGLUT1 (SLC17A7) For: ACTCCATACACCTCTAGCCTGA, Ta = 59.75 °C;
VGLUT1 (SLC17A7) Rev: AGGGAGGACTTGCATCTTAAGC, Ta = 60.09 °C;
SYT1 For: GCAGTGGTATGATGAAGGGCA, Ta = 52.41 °C;
SYT1 Rev: CAGTTTCCAGCCATGCATTCC, Ta = 52.38 °C;
SYT2 For: CCCTCTGCCACCATGAGAAA, Ta = 59.67 °C;
SYT2 Rev: TGTAGAGTTGTCGGCAGGTG, Ta = 59.68 °C;
SYB1 For: AGTGTTCGCTTTCATGTGGC, Ta = 59.41 °C;
SYB1 Rev: GGCCATCTTCACATCGGACA, Ta = 60.11 °C;
STX1 For: CCTTTTCCCTCCCATCCCAC, Ta = 60.03 °C;
STX1 Rev: AGATCATGCACACGACACGG, Ta = 60.74 °C;
VAMP2 For: CTGCACCTCCTCCAAACCTT, Ta = 59.89 °C;
VAMP2 Rev: CAGCTCCGACAACTTCTGGT, Ta = 59.97 °C;
GRIA1 For: AGTGGCAGTGGAGAGAATGG, Ta = 59.38 °C;
GRIA1 Rev: AGGGAATGGATTGCATGGACT, Ta = 59.43 °C;
GAPDH For: GGCATCGAAGGTGGAAGAGT, Ta = 59.75 °C;
GAPDH Rev: GGCATCTTGGGCTACACTGA, Ta = 59.75 °C;
PPIA For: TCCTGGCATCTTGTCCATGG, Ta = 59.74 °C;
PPIA Rev: TTCAGTCTTGGCAGTGCAGA, Ta = 59.53 °C;
RPL13A For: TCCGATAGTGCATCTTGGCC, Ta = 59.89 °C;
RPL13A Rev: AAGTACCAGGCAGTGACAGC, Ta = 59.96 °C.

Relative quantification of PRRT2 expression was made using the 2-ΔΔCt method (Pfaffl, 2001), normalizing data to the geometric mean of three housekeeping transcripts (GAPDH, PPIA, RPL13A).

2.5. Histology and immunofluorescence

Animals were anesthetized with an intraperitoneal injection of urethane and transcardially perfused with ice-cold 4% paraformaldehyde in 0.1 M phosphate buffer (PB; pH 7.4). After perfusion, brains were dissected and kept in the same fixative solution overnight at 4 °C. After several washes in 0.1 M PB, brains were then cryoprotected by immersion in 10, 20 and 30% sucrose solutions and subsequently cut in 30 μm sections with a cryostat and stored at −20 °C in a solution containing 30% ethylene glycol and 20% glycerol in 0.1 M PB. Cryosections were then washed in phosphate-buffered saline (PBS, pH 7.4) and processed for free-floating immunofluorescence. After blocking step in PBS containing 0.05% Triton X-100 and 10% normal goat serum (NGS), sections were incubated overnight at room temperature with the following primary antibodies: mouse ant-NeuN (1:500, Millipore), rabbit anti-VGAT (1:300, Synaptic System), mouse anti-VGLUT1 (1:250, Synaptic System). Antibodies were diluted in PBS with 3% of NGS and 0.05% Triton X-100. Double immunofluorescence was performed with the simultaneous addition of the primary antibodies. Sections were then washed in PBS (4 × 10 min) and incubated for 1 h at 25 °C with anti-rabbit Alexa Fluor 488 and anti-mouse Alexa Fluor 568 (Invitrogen). After several PBS rinses, sections were mounted on glass slide and observed with a Leica SP8 confocal microscope (Leica Microsystem). Images were acquired using the multi-track mode to avoid fluorescence crosstalk (pinhole: 1.0 airy unit). For the quantitative analysis of VGAT and VGLUT1 puncta, *Z*-series stacks of seven consecutive confocal sections (1024 × 1024 pixels) spaced by 2 μm were acquired at 40×. Images from both channels were overlaid and background labeling was subtracted. Fluorescence levels were analyzed on confocal images by measuring pixel intensity using the Fiji software. Both VGAT and VGLUT1 positive puncta were calculated using the Fiji software. Histology was performed on the left hemisphere on neurons labeled with anti-NeuN mouse primary antibody/anti-mouse Alexa Fluor 488 secondary antibody. Frontal, medial and caudal sections were chosen to calculate cortex and corpus callous thickness. Medial and caudal sections were used to analyze the thickness of both CA1 and CA3 pyramidal cell layer and *stratum radiatum*. In the same section, both granule cell layer and molecular layer thickness of the DG were analyzed. Images from the cerebellum were always acquired from the fourth/fifth lobe to measure the thickness of granule cell and molecular layers. Images were acquired at 10× and all parameters were analyzed using the Fiji software.

2.6. Behavioral analysis

Behavioral experiments were conducted during the standard light phase, between 11.00 a.m. and 6 p.m. All mice were obtained from HET × HET matings and three cohorts of mice were used for motor behavior, cognitive tests and PTZ treatment. For motor assessment, the order of testing was as follows: (1) spontaneous behavior and righting reflex in mouse pups; (2) open field; (3) accelerating Rotarod; and (4) footprint test in adult mice. For the experiments in the postnatal phase, male and female mouse pups were tested, but since no differences were detected between gender, data were collapsed across sex. Cognitive tests and audiogenic stimulation were assessed in 2-months old male mice and the order of testing was as follows: (1) novel object recognition; (2) fear conditioning; and (3) audiogenic seizures. A third cohort of 2 months old mice was used for the PTZ experiment.

2.6.1. Spontaneous movements in mouse pups

For the analysis of spontaneous movements, mouse pups were video-recorded for 3 min at P4, P8, P12 and P16. On the day of testing, each pup was placed into an empty standard cage located inside a sound-attenuating styrofoam box, and assessed for spontaneous behavior during a 3-min test. At the end of experimental session on the first day of test, pups were tattooed (Ketchum permanent Tattoo Inks green paste, Ketchum Manufacturing Inc., Brockville ON Canada) on the paw for a subsequent recognition (Romano et al., 2013). For the analysis of spontaneous movements, frequency and duration of behavioral items were analyzed by an observer blind to mouse genotype. We used the StatView script to manually score the following behavioral

patterns: locomotion (general translocation of the body of at least 1 cm in the glass container), face washing (forepaws moving back and forth from the ears to the snout and mouth), wall climbing (alternating forelimb placing movements on the wall of the container), pivoting (locomotor activity involving the front legs alone and resulting in laterally directed movements), circling (circular locomotor activity involving the all legs and resulting in laterally directed movements), curling (roll, vigorous side-to-side rolling movements while on the back), bouncing (short body jerks when the animal is placed with the four paws on the floor), loss of balance (the animal loses control at least of one of the four paws) and backward locomotion (the animal performs at least backward two steps with all four paws).

2.6.2. Righting reflex in mouse pups

After each recording session, each pup was placed on its back over a flat surface, and the time needed to return to the natural position (all four paws on the floor) was measured. The reflex was tested once with a cut-off latency of 60 s.

2.6.3. Somatic growth in mouse pups

At the end of the recording sessions and righting reflex test, each pup was measured for body weight, body length, tail length and its axillary temperature measured by gentle insertion of the thermal probe (digital thermometer with microprobe; Stoelting Co., IL) in the skin pocket between upper foreleg and chest of the animal for about 30 s.

2.6.4. Open field test

To evaluate both locomotor activity and anxiety-like behaviors in 2-months-old male mice, each subject underwent an open field test. Mice were individually placed in an opaque open field box (40x40x40 cm) with the Anymaze camera (Stoelting) mounted 20 cm above the apparatus. The session started by placing the animal in the center of the arena for 10 min (habituation), followed by 20 min of test. The floor of the apparatus was cleaned with 50% ethanol after each test. Total distance, time locomotion, time immobile, mean speed, as well as time in the center and in the border were automatically collected using the Anymaze activity monitor and analyzer software system. Manual scores using StatView software were conducted to analyze the following behaviors: grooming, wall rearing, jumping, loss of balance events and backward locomotion.

2.6.5. Accelerating Rotarod

A Rotarod apparatus (Basile, Comerio, Italy) was used to measure the mouse's balance and motor coordination at two months of age. Each mouse was tested for three trials with the rate of rotation increasing from 4 to 40 rpm during 3 min (De Filippis et al., 2010). The trial ended when the mouse fell from the rod (3 cm diameter) or remained on the Rotarod for at least 180 s, whichever event occurred first. The time spent on the Rotarod was recorded by an automated unit, which automatically stopped as the mouse fell. The mouse was placed back in its home cage for a minimum of 10 min between each trial.

2.6.6. Footprint test

To obtain footprints, the hind- and fore- feet of the mice were coated with red and green nontoxic paints, respectively. The animals were then allowed to walk along a 100-cm long, 10-cm wide runway (with 10-cm-high walls) into an enclosed box and a sheet of millimeter paper was placed on the floor of the runway. To characterize the walking pattern of each mouse, the average distance between each stride (stride length, SL), the distance between left and right hind footprints (hind-base width, HB) and the distance between left and right fore footprints (fore-base width, FB) were measured (Capoccia et al., 2015).

2.6.7. Novel object recognition

The novel object recognition test was conducted in the open field arena. The test consisted of two habituation sessions (day 1 and 2), a 10-min familiarization session (day 2), and a 5 min recognition test (day 2) as previously reported (Yang et al., 2012). During the 10-min. Familiarization session, two different objects were placed in the arena. The objects used during the task were different in shape, color, size, and material (glass, plastic). One hour after the familiarization session, a 5-min novel recognition test started. One clean familiar object and one clean novel object were placed in the arena, where the two previous objects had been located during in the familiarization phase. The familiarization sessions and the recognition test were videotaped and automatically scored by the Anymaze software. Object investigation was defined as the time spent in contact with the object. Recognition memory was defined as spending significantly more time sniffing the novel object than the familiar object. Time spent sniffing two identical objects during the familiarization phase confirmed the lack of an innate side bias.

2.6.8. Contextual and cue fear conditioning

The contextual and cue fear-conditioning test was conducted in 40x40x40 cm arenas located inside a sound-attenuating styrofoam box, as described (Scattoni et al., 2013). Training and conditioning tests took place in two identical arenas calibrated to deliver identical foot shocks. When placed in the chamber, the grid floor connected with a circuit board for delivery of a scrambled electric shock. A camera mounted on the front door of the environmental chamber recorded test sessions, which were automatically scored using the Anymaze software. During the training session, the mouse was placed in the test chamber and allowed to explore freely for 2 min. A pure tone (5 kHz, 80 dB) serving as the conditioning stimulus (CS) was played for 30 s. During the last 2 s of the tone, a foot shock (0.5 mA) was delivered as the unconditioned stimulus (US). Each mouse received three CS-US pairings, separated by 90 s intervals. After the last pairing, the mouse was left in the chamber for another 2 min, during which freezing behavior was scored. Contextual conditioning was tested 24 h later in the same chamber, but without foot shock. Each mouse was placed in the chamber for 5 min in the absence of CS and US, during which freezing behavior was scored. The mouse was then returned to its home cage. Cued conditioning was conducted 2 h after training. Contextual cues were altered by covering the grid floor with a smooth grey plastic sheet and by replacing the black arena with a new transparent one. The session consisted of a 2 min free exploration period, followed by 1 min of the identical CS tone (5 kHz, 80 dB) and 2 more min of free exploration. Freezing behavior was scored during all segments of the test. The chamber was thoroughly cleaned of odors between sessions, using 50% ethanol and water.

2.6.9. Audiogenic seizures

The test was conducted in a circular apparatus (15 cm diameter) located inside a Startle Response/PPI test system chambers (TSE Systems GmbH, Germany) as described (Deidda et al., 2015). The session consisted of a 2-min free exploration period, followed by 1-min acoustic stimulation (white noise at 120 dB) and 2 more min of free exploration. All sessions were recorded with a digital camera (Logitech, HD Professional Webcam C920) angled 60° from above to optimize behavioral analysis. The audiogenic responses were scored manually as: 0, no response; 1, wild running; 2, jumping; 3, tonic-clonic seizure. The test was conducted between 03:00 p.m. and 05:00 p.m. to avoid possible circadian variations and animals were tested only once.

2.6.10. Pentylenetetrazol-induced seizures

WT and KO littermates implanted for EEG monitoring (see below) were repeatedly injected with unitary doses of PTZ (10 mg/kg intraperitoneally in 0.9% saline) every 10 min and continuously monitored after each injection in a 17 × 17 × 25 cm box equipped with the Anymaze video tracking system. Seizure scoring was conducted as previously reported by Browning and Nelson (1986), and the following parameters were considered: (i) myoclonic jerk, (ii) face and forelimb clonus (iii) whole body clonus with twisting or loss of posture, (iv) running/

bouncing clonus, (v) tonus: (tonic flexion and tonic extension) (Browning and Nelson, 1986). At the end of the observation period, animals were killed humanely by cervical dislocation. Seizure manifestations were recorded by inspection of the videos by two independent observers blind to the genotype. Threshold dose (mg/Kg) for induction of seizures, as well as latency (s) and duration (s) of induced seizures were computed as previously described (McLeod et al., 2013; Rantala et al., 2015). An integrated measure of seizure propensity was calculated, for each animal, as follows: [seizure duration]/([seizure latency] × [threshold dose]) × 100. The total covered distance and duration of freezing events in the pre-seizure doses were automatically assessed using the Anymaze software.

2.7. Electroencephalography

Mice tested to assess the threshold for paroxysmal events were implanted for wireless electroencephalogram (EEG) recordings. An EEG transmitter [A3019D, Open Source Instruments; (Chang et al., 2011)] was implanted subcutaneously with a subdural intracranial recording electrode (Bregma −2.00 mm; Lateral 2.00 mm). A reference electrode was implanted in the cerebellum (Bregma −5.80 mm; Lateral 1.00 mm). All surgeries were conducted as previously described (Chang et al., 2011). Animals were housed separately in Faraday cages, and EEG was recorded the day of the experiment. EEG was processed with the Neuroarchiver tool (Open Source Instruments), which determined EEG power for different frequency bands. The trace was centered around 0 V by subtraction of the average. Short (<100 ms), high-amplitude artifacts exceeding 5× root mean square ('glitches') detected by threshold and periods with failed transmission were high pass–filtered at 10 Hz.

2.8. Patch-clamp recordings in hippocampal and cerebellar slices

Acute hippocampal and cerebellar slices were prepared from 4 to 8 weeks-old WT and PPRT2 KO littermates with the genotype blind to the experimenter. Mice were anesthetized by a brief exposure to isoflurane, decapitated and the brain rapidly dissected in an ice-cold cutting media containing (in mM): 87 NaCl, 25 $NaHCO_3$, 2.5 KCl, 0.5 $CaCl_2$, 7 $MgCl_2$, 25 glucose, 75 sucrose and saturated with 95% O_2 — 5% CO_2. Coronal and sagittal slices (350 μm) were obtained from the hippocampus and cerebellum, respectively, with a Microm HM 650 V microtome equipped with a Microm CU 65 cooling unit (Thermo Fisher Scientific, Waltham, MA) to maintain the cutting-media at low temperature (2–5 °C) while slicing. Before starting the recordings, slices were allowed to recover for 30–45 min at 35 °C in a constantly 95% O_2 — 5% CO_2 bubbled recording artificial cerebrospinal fluid (ACSF) solution containing (in mM): 125 NaCl, 25 $NaHCO_3$, 25 glucose, 2.5 KCl, 1.25 NaH_2PO_4, 2 $CaCl_2$ and 1 $MgCl_2$. Following recovery, slices were kept at room temperature for the rest of the experimental day. For all experiments on glutamatergic transmission, a high K-gluconate intracellular solution was used (containing in mM: 126 K-gluconate, 4 NaCl, 1 $MgSO_4$, 0.02 $CaCl_2$, 0.1 BAPTA, 15 glucose, 5 HEPES, 3 MgATP, and 0.1 NaGTP, pH 7.3, 290 mosmol/l), while a high-chloride intracellular solution (containing in mM: 126 KCl, 4 NaCl, 1 $MgSO_4$, 0.02 $CaCl_2$, 0.1 BAPTA, 15 glucose, 5 HEPES, 3 MgATP and 0.1 NaGTP, pH 7.3, 290 mosmol/l) was used for the investigation of GABAergic transmission. QX314 (10 mM) was also added to the intracellular solution for ePSC recordings. Patch-clamp experiments were performed with borosilicate pipettes, pulled with a Narishige PC-10 vertical puller to a final resistance of 3–4 mΩ, using the Multiclamp 700B or AxoPatch 200B amplifier (Molecular Devices, Sunnyvale, CA). Data were acquired with a 2 kHz low-pass Bessel filter and digitized at 10 kHz with Clampex 10.2 and analyzed offline with Clampfit 10.2 (pClamp, Molecular Devices, Sunnyvale, CA), MiniAnalysis (Synaptosoft, Decatur, GA) and Origin (OriginLab, MA). Extracellular stimulation to evoke PSCs was performed with a monopolar glass electrode (intensity: 10–100 mA, duration: 5–10 μs) filled with ACSF and connected with an isolated pulse stimulator (A-M Systems, Carlsborg, WA). The criteria used to define the extracellular stimulation were: (1) no failures in response to repeated 0.1 Hz stimulation; (2) postsynaptic responses at least three-fold higher than the square root of noise; (3) latency and shape of synaptic current remained invariant. After finding a cell that met these criteria, we continued all the experiments at stimulation intensity 10% higher than the minimal needed, to avoid possible failures.

2.8.1. Hippocampus

Whole-cell recordings were performed on visually identified dentate gyrus (DG) granule cells (GCs) as previously described (Medrihan et al., 2013). We recorded mature GCs with R_m < 300 MΩ at a holding potential of −70 mV in which PSCs were evoked by stimulation of the medial perforant path. Evoked excitatory postsynaptic current (eEPSC) recordings were recorded in the presence of SR95531 (10 μM), CGP 55845 (5 μM) and D-AP5 (50 μM), while evoked inhibitory postsynaptic current (eIPSC) recordings were performed in the presence of D-APV (50 μM), NBQX (20 μM) and CGP 55845 (5 μM) (all from Tocris Bioscience, Ellisville, MO). For recordings of miniature EPSCs/IPSCs, 0.3 μM TTX was added to the recording solution.

2.8.2. Cerebellum

Whole-cell recordings were obtained from Purkinje cells (PCs) that were voltage-clamped at −60 mV with 60–80% RS compensation, as previously described (Valera et al., 2012) with some modifications. eEPSCs were elicited by parallel fibers electrical stimulation *via* a glass stimulation pipette placed in the molecular layer > 100 μm away from the recorded cell to avoid the direct stimulation of the dendritic tree. To avoid plasticity, trains of parallel fibers stimulation were applied in the presence of the CB1 receptor antagonist AM251 (1 μM), the specific mGluR1 receptor antagonist JNJ16259685 (1 μM), the pre-/post-synaptic $GABA_B$ receptor antagonist CGP55845 (3 μM). D-APV (100 μM) and SR95531 (10 μM) were also added to the recording solution. mEPSCs were recorded in presence of SR95531 (5 μM), CGP55845 (3 μM) and TTX (0.3 μM).

2.9. Statistical analysis

Data are expressed as means ± SEM for number of cells throughout. Normal distribution of data was assessed using the D'Agostino-Pearson's normality test. The F-test was used to compare variance between two sample groups. To compare two normally distributed sample groups, the two-tailed unpaired Student's *t*-test was used. To compare more than two normally distributed sample groups, one- or two-way ANOVA was used, followed by the Bonferroni's, Dunnett's or Fisher PLSD test. The occurrence of a given behavioral trait in the mouse population was evaluated using the Fisher exact test. A value of $p < 0.05$ was considered significant. Statistical analysis was carried out using OriginPro-8 (OriginLab Corp., Northampton, MA, USA), StatView 5.01 (SAS Institute, Inc.) and Prism (GraphPad Software, Inc.) software.

3. Results

3.1. Characterization of PRRT2 KO mice

After the demonstration that successful homologous recombination had occurred in our PRRT2 mice by PCR (Fig. S1B), we confirmed the creation of a null allele for PRRT2 by analyzing the expression of PRRT2 protein in various brain areas in adult WT, HET and KO mice by quantitative immunoblotting (Fig. S1C). In agreement with the previous report (Valente et al., 2016), PRRT2 protein was highly expressed in several areas of the WT brain, including cerebellum, frontal, sensory and visual cortices, hippocampus, striatum and brain stem. In KO mice, the immunoreactive 68 kDa PRRT2 band was totally undetectable by western blotting in fractions from any of the brain regions analyzed, while

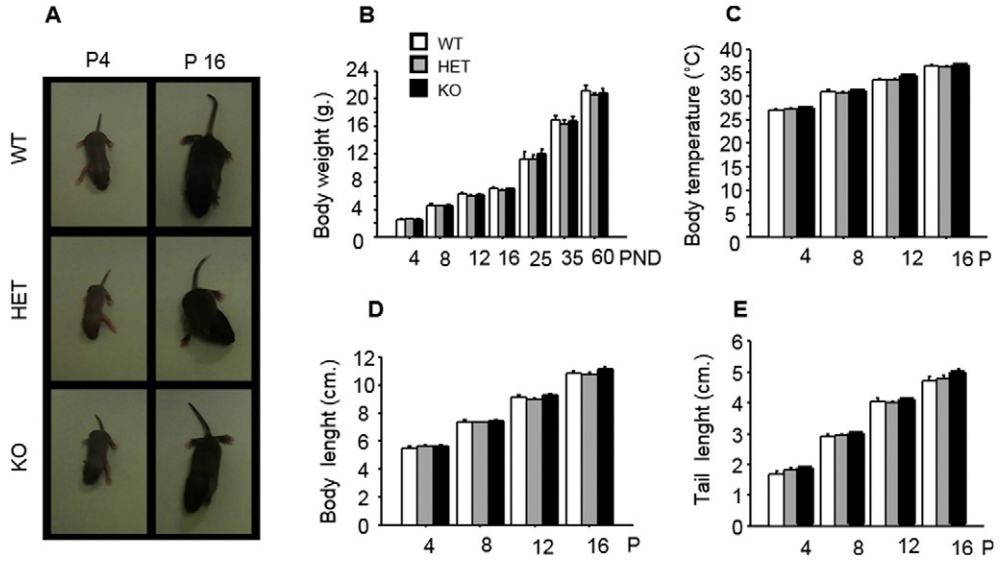

Fig. 1. Somatic growth during postnatal development. A. Representative picture of WT, HET and KO PRRT2 mouse pups at P4 and P16. B–E. Analysis of the markers of somatic growth revealed no differences between WT, HET and KO mice during development on body weight (B), body temperature (C), body length (D) and tail length (E). Data (means ± SEM) were obtained from cohort 1 (10 litters): N = 15 WT, 43 HET and 17 PRRT2 KO. Two-way ANOVA and post-hoc Fisher PLSD test.

PRRT2 expression was approximately halved in all regions of HET brains (Fig. S1C).

Offspring of HET mice, genotyped by PCR, were found to follow the expected Mendelian distribution and no prenatal lethality was observed. The somatic growth and general health status in KO animals were indistinguishable from those observed in both HET and WT littermates, with normal somatic growth in terms of body weight, body temperature, body length and tail length over postnatal development (Fig. 1A–E).

Although the brain gross structure appeared comparable in the three genotypes, we performed a morphometric analysis at various rostrocaudal levels based on NeuN immunoreactivity. Intriguingly, the thickness of the neocortex in young adult PRRT2 KO mice was significantly reduced in medial and caudal regions compared to their WT controls, in the absence of changes in cortical thickness in frontal regions and in the thickness of the corpus callosum at all levels analyzed (Fig. 2A–C). Moreover, no significant differences were observed in the thickness of the CA1, CA3 and DG regions of the hippocampus, as well as for the molecular and granule layers of the cerebellum (Fig. S2).

3.2. Regional expression of PRRT2

We used β-gal activity to follow the precise regional and cellular expression pattern of PRRT2 in the mutant mice. We analyzed the rostrocaudal expression pattern of β-gal in coronal sections from the brain and spinal cord of HET and KO mice at various postnatal times and in young adults (Fig. 3).

On a macroscopic level, β-gal appeared strongly expressed in the cerebellum and hindbrain with respect to more rostral areas (Fig. 3A). Examination of the entire nervous system from mutant mice confirmed an average low expression level of β-gal in the forebrain, but with hot spots of expression in restricted areas. The analysis of rostral sections revealed high expression levels in layer VIb of the neocortex, septal nuclei and claustrum (Fig. 3B). At more caudal levels, the β-gal signal was high in the hippocampus, particularly in the hilus, DG and CA3, with lower β-gal activity in the CA1, CA2 areas (Fig. 3C, D). Specific signals were also observed in the amygdala, collicula and periaqueductal grey (Fig. 3D). In more caudal sections, a strong expression of PRRT2 was detected in the granular layer of cerebellum, whereas PCs and the molecular layer were negative except for sparse positive interneurons in the latter. A faint staining was also detected in the medulla oblongata at the level of the vestibular nuclei (Fig. 3E). Finally, PRRT2 expression was observed in the spinal cord, with intense β-gal staining in the *substantia gelatinosa* as well in the dorsal horn (Fig. 3F). No β-gal staining was present in the white matter, confirming the neuron-specificity of PRRT2 expression. PRRT2 expression was very low at postnatal day (P) 4 and 8, while at P16 its expression markedly increased, with a regional distribution similar to the adult (not shown). This finding agrees with our previous study in which we found that PRRT2 mRNA, low at birth, increases postnatally over the first month of life (Valente et al., 2016).

To assess the specificity of the PRRT2-promoter driven expression of β-gal, we compared the mRNA levels of PRRT2 and β-gal in three major areas of WT, HET and KO brains, namely frontal cortex, hippocampus and cerebellum, characterized by significantly different β-gal activities (Fig. 3G). This analysis confirmed that in WT brains the cerebellum has much higher levels of PRRT2 transcript than cortical areas, and that the expression levels are reduced to approximately 50% in HET brains and virtually absent in KO brains. Accordingly, the parallel quantification of the LacZ transcript in the three genotypes revealed progressively increasing expression levels in HET and KO brains, with a cerebellum/cortical expression ratio similar to that observed for PRRT2 mRNA in HET and WT brains, respectively (Fig. 3G). The comparison of the expression of PRRT2 protein in various brain areas (Fig. S1C) with the mapping of β-gal/PRRT2 transcript reveals the existence of mismatches, particularly at the level of the cortex and the striatum that exhibit low levels of cellular transcript, but high expression of PRRT2 protein.

3.3. Behavioral phenotyping of the PRRT2 mouse line

3.3.1. Spontaneous motor behavior and righting reflex in PRRT2 mouse pups

In this test a significant genotype effect was observed in bouncing behavior ($F_{2,210} = 4.684$, $p = 0.01$; Fig. 4A) and an interaction genotype × day in the loss of balance ($F_{6,210} = 2.265$, $p = 0.03$; Fig. 4B), backward locomotion ($F_{6,210} = 5.432$, $p = 0.0001$; Fig. 4C) and grooming ($F_{6,210} = 2.792$; $p = 0.01$, Fig. 4D), while no differences were found in the other parameters analyzed (Fig. 4E). Interestingly, post-hoc tests revealed a higher frequency of abnormal events in KO mice when compared to HET and WT starting from P8, a crucial window for motor development, since at this time point animals start moving all four paws on the floor (see circling and locomotion in Fig. 4E). PRRT2 KO

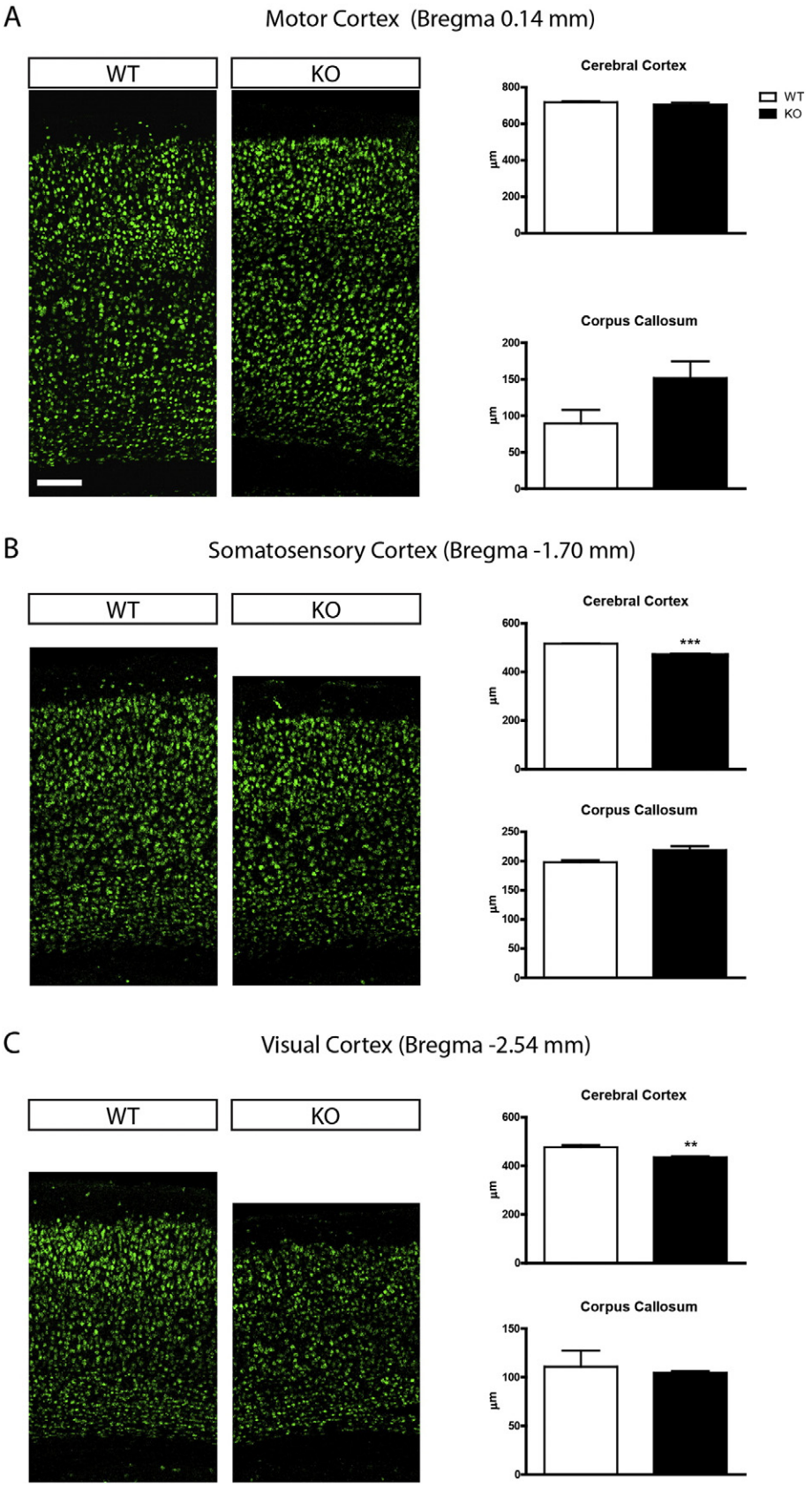

Fig. 2. Gross brain histology of cerebral cortex and corpus callosum. Representative confocal images of NeuN staining (green) in the motor (A), somatosensory (B) and visual (C) cortices of WT and PRRT2 KO mice and the respective morphometric analysis of the thickness of both cortex and corpus callosum. Data are expressed as means ± SEM; $^{**}p < 0.01$, $^{***}p < 0.001$; two-tailed unpaired Student's *t*-test. N = 3 for both WT and KO mice. Scale bar, 100 µm.

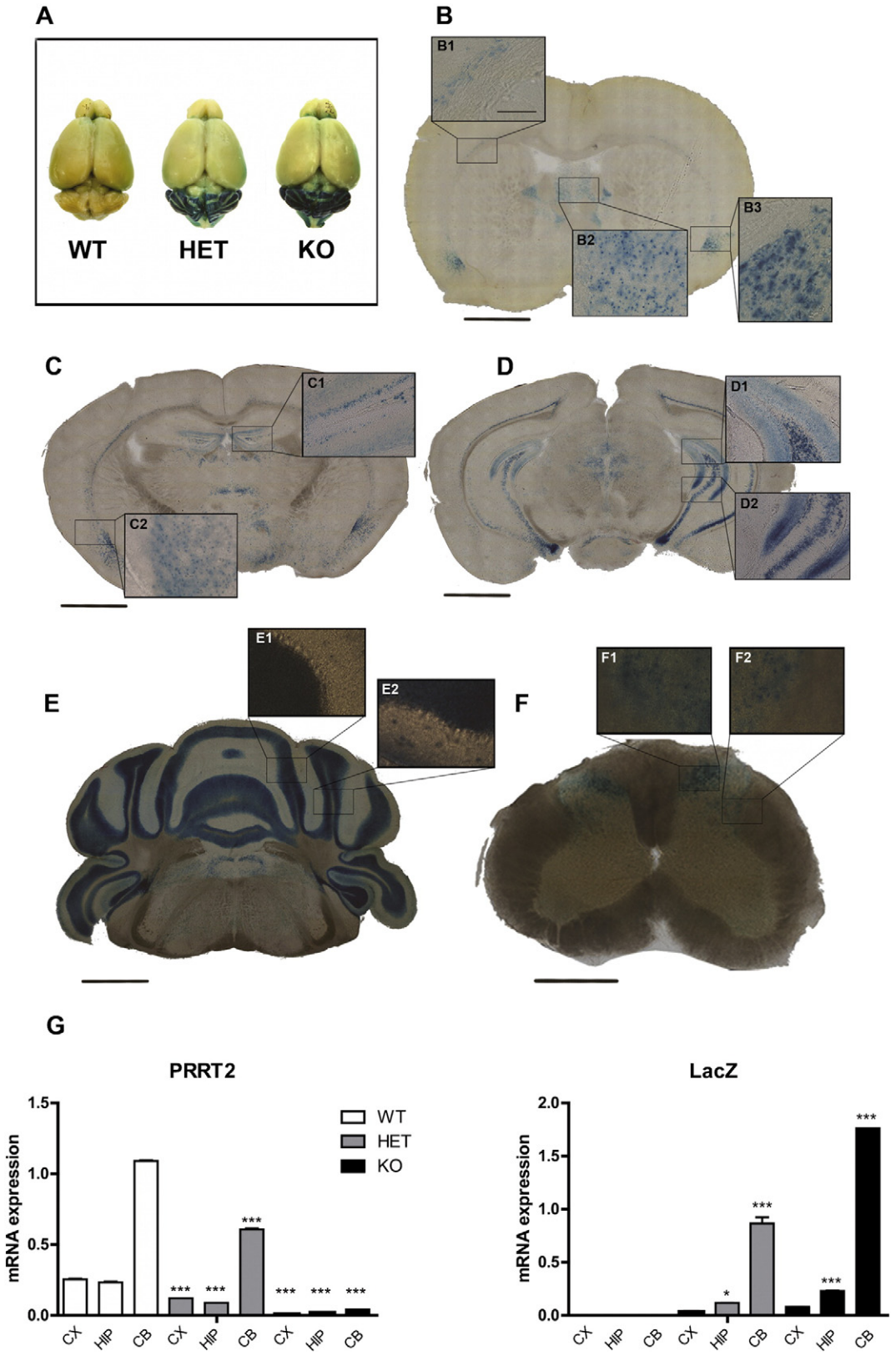

Fig. 3. β-gal activity in the CNS of adult PRRT2 KO mice. A. Representative picture of β-gal staining in isolated adult brains from WT, HET and KO PRRT2 mice. A strong expression of β-gal was evident in the cerebellum of HET and KO mice, while WT mice were negative. B. PRRT2 was expressed in layer VIb of the neocortex (B1), septal nuclei (B2) and claustrum (B3). C, D. PRRT2 was expressed in hippocampal regions, particularly DG, hilus and CA3 (C1, D1, D2). Thalamic regions, amygdala (C2), periaqueductal grey, superior colliculus and neocortical layer VIb were also positive. E. A strong expression of PRRT2 was present in the cerebellum, particularly in the granular cell layer, while Purkinje cells were negative (E1). In the molecular layer, only sparse interneurons were positive (E2). F. An intense PRRT2 expression was present in the *substantia gelatinosa* and the dorsal horn of the spinal cord (*F*1-F2). Scale bars: 2 mm (B-D), 1 mm (E, F) and 0.1 mm (insets). N = 3 PRRT2 KO mice. G. Quantitative analysis of PRRT2 (left) and LacZ (right) mRNA levels (means ± SEM) in the cortex (CX), hippocampus (HIP) and cerebellum (CB) of WT, HET and KO mice by qRT-PCR. $^{*}p < 0.05$, $^{***}p < 0.001$, one-way ANOVA and post-hoc Bonferroni's test. Samples were run in triplicate from N = 3 for both WT and KO mice.

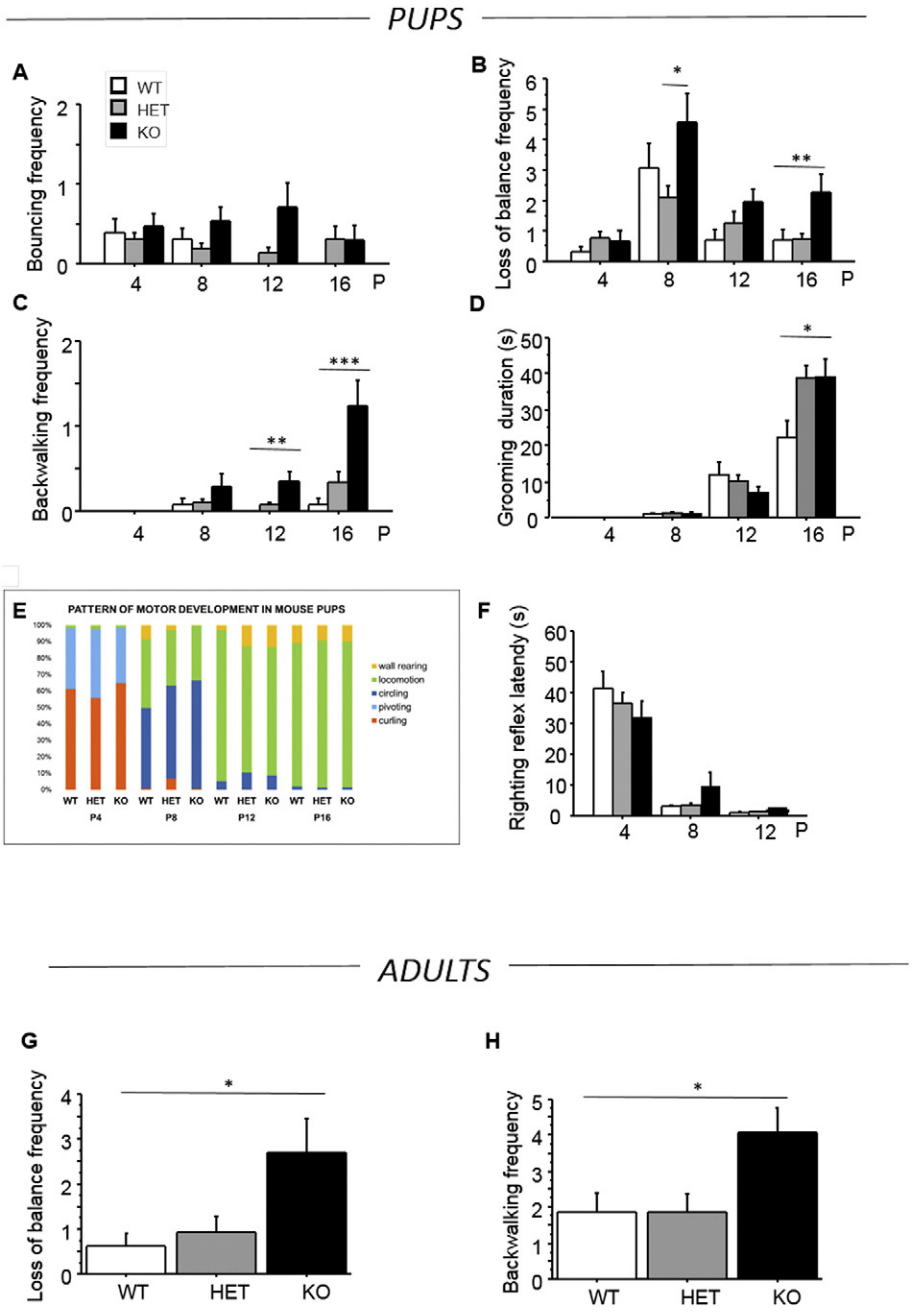

Fig. 4. Motor behavioral patterns shown by PRRT2 mouse line during postnatal development and at adulthood. A–D. A higher frequency of bouncing (A), loss of balance (B), back walking (C) and a longer duration of grooming (D) were observed in KO mouse pups as compared with HET and WT littermates during 3-min maternal separation at P4, P8, P12 and P16. E. The panel represents the percentage of time spent by WT, HET and KO pups performing the various behaviors analyzed at P4, P8, P12 and P16. F. Righting reflex latencies measured at the end of the maternal separation test. N = 14 WT, 43 HET and 17 KO mouse pups. G–H. A higher frequency of loss of balance (G) and back walking (H) was still present in adult PRRT2 KO mice. N = 8 WT, 14 HET and 13 KO male mice. All data are expressed as means ± SEM; *p < 0.05, **p < 0.01, ***p < 0.001; two-way ANOVA and post-hoc Fisher PLSD test.

mice experienced loss of balance with high frequency at P8 and started to display backward locomotion (moonwalking) at P12. The most critical picture was seen at P16, when a mature motor profile was reached by all three genotypes with locomotion and wall climbing behaviors (see Fig. 4E). At this time point, post-hoc tests confirmed a higher frequency of balance loss, backward locomotion and grooming duration in KO mice when compared to either WT or HET mice. Interestingly, at P12 and P16, the presence of bouncing persisted in HET and KO mice, but not in WT littermates. Given the motor abnormalities observed during spontaneous behavior, we investigated the righting reflex that requires a complex coordination between head, trunk, and paws (Fig. 4F). We limited the analysis to the developmental milestones of the righting reflex, to avoid stressful manipulations that could potentially trigger motor paroxysms. No genotype differences were found in the righting reflex latency, suggesting a normal motor coordination development in PRRT2 mouse line (Fig. 4F). Altogether, our screening in PRRT2 KO mouse pups uncovered the presence of paroxysms, namely bouncing and back walking, together with uncontrolled grooming, in spite of the presence of a physiological pattern of motor development.

3.3.2. Spontaneous and evoked motor behavior in PRRT2 adult mice

At adulthood, we found a genotype effect for loss of balance (genotype effect $F_{2,32} = 3.903$, $p = 0.03$; Fig. 4G) and backward locomotion (genotype effect $F_{2,32} = 4.658$, $p = 0.01$; Fig. 4H; Movie S1), with no differences in grooming and locomotion (Fig. S3A–C). No significant genotype-specific differences were also observed when the time spent by the

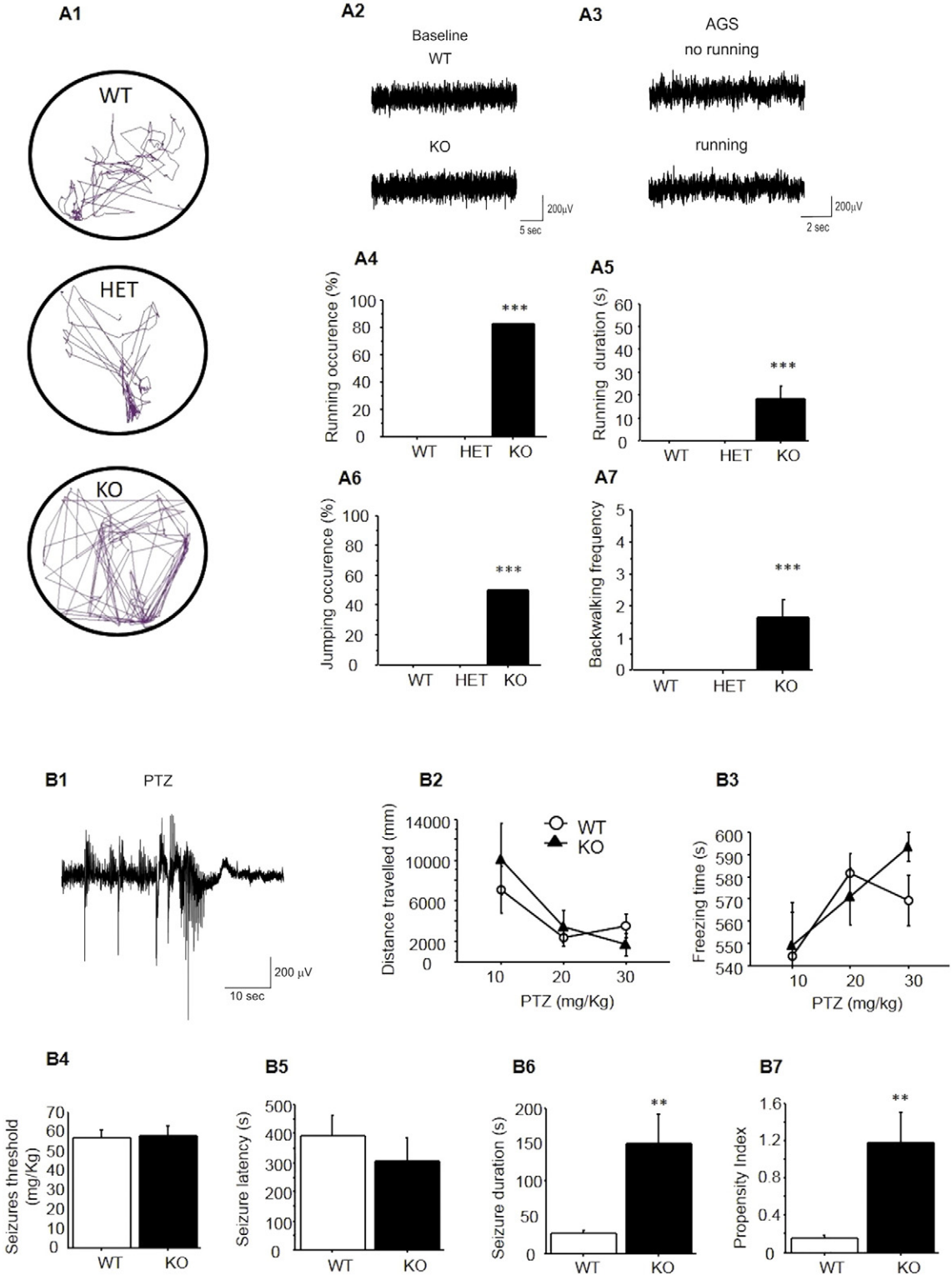

Fig. 5. Paroxysmal phenotype of PRRT2 KO mice. A. Motor paroxysms in response to audiogenic stimuli. A1. Representative trackings of WT, HET and KO mice during 1-min exposure to an audiogenic stimulus (white noise, 120 days; A1). A2. EEG recorded in WT and PRRT2 KO mice during the resting adaptation period. A3. Representative EEG traces of PRRT2 KO mice during the audiogenic response before and during wild running. A4–A7. The plots show the percentage of animals responding with wild running to the audiogenic stimulus (A4), the mean duration of wild running (A5), the percentage of animals performing jumps (A6) and the frequency of back walking performed during the audiogenic response (A7) as means ± SEM. N = 6 WT, 7 HET and 6 KO male mice. B. Pentylenetetrazol-induced seizures. A 10-s representative EEG trace of a PRRT2 KO mouse recorded during a PTZ-induced tonic-clonic seizure is shown (B1). The plots (means ± SEM) depict: the total distance covered (B2) and the duration of the immobility/freezing episodes (B3) collectively recorded at subthreshold PTZ doses (10, 20 and 30 mg/kg); the threshold for provocation of the first tonic-clonic seizure (B4); the seizure latency from the administration of the threshold doses (B5); the duration of the first tonic-clonic seizure (B6); and the compound seizure propensity index (B7) calculated as described in the Materials and Methods. Statistical analysis was performed using the Fisher exact test (A4, A6) and two-way ANOVA and post-hoc Fisher PLSD test (A5, A7, B2–B7). $^{**}p < 0.01$; $^{***}p < 0.001$. N = 6 WT, 7 HET and 6 KO (A); 7 WT and 6 KO (B).

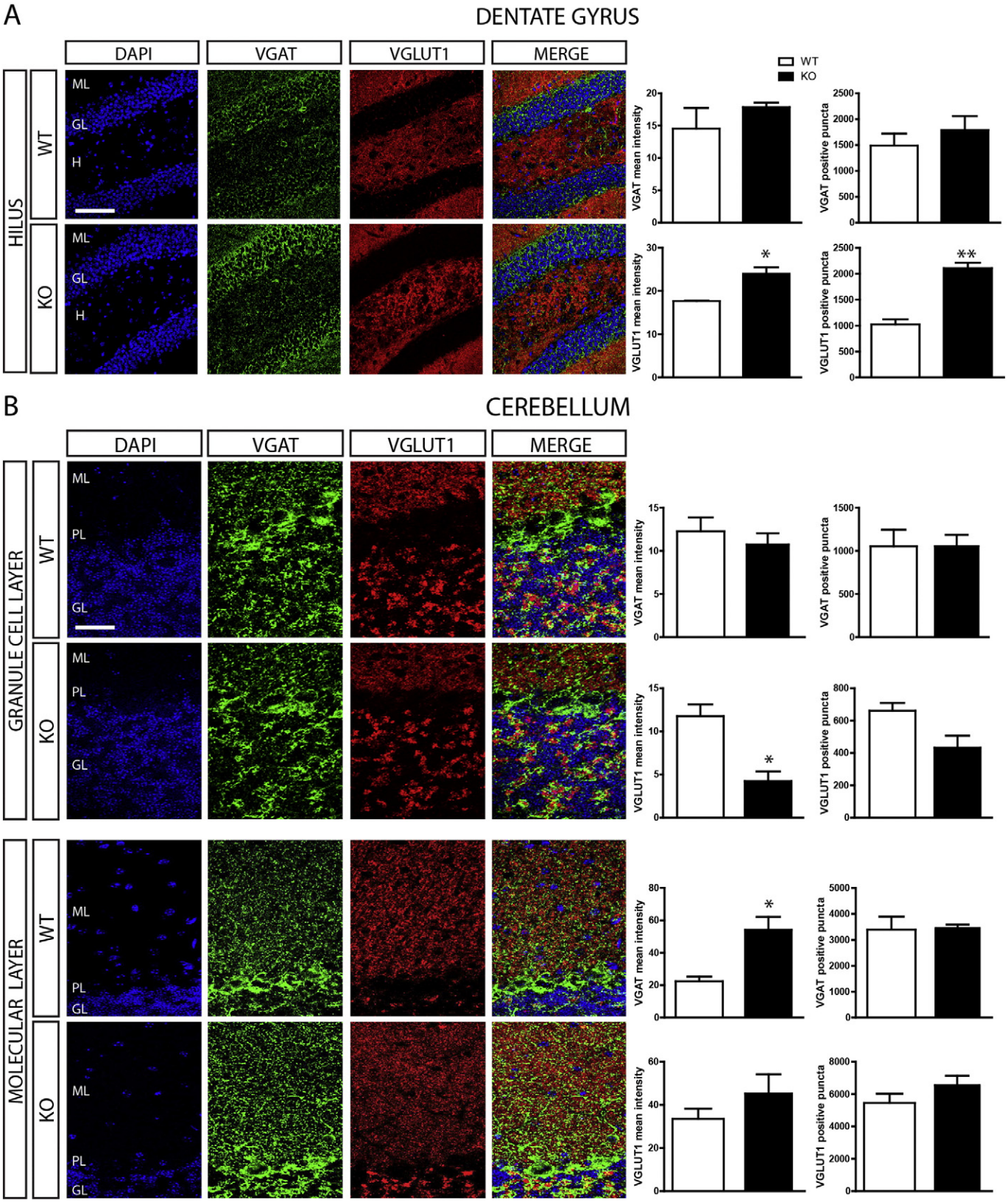

Fig. 6. Expression of synaptic markers in PRRT2 KO mice. Representative confocal images of the hilus of the DG (A) and of the granule cell (upper panel) and molecular (lower panel) layers of the cerebellum (B) of WT and PRRT2-KO mice stained with DAPI (blue), VGAT (green), VGLUT1 (red) and their merge. Histograms on the right show the mean intensity VGAT and VGLUT1 immunoreactivities and the number of VGAT- and VGLUT1-positive puncta. (ML: molecular layer; GL: granule cell layer; H: Hilus; PL: Purkinje cell layer). All data are expressed as means ± SEM; $^{*}p < 0.05$, $^{**}p < 0.01$; two-tailed unpaired Student's *t*-test. N = 3 for both WT and KO. Scale bar, 150 μm.

Table 1
Expression levels of synaptic proteins transcripts in the cortex, hippocampus and cerebellum of the PRRT2 mouse line.
The mRNA expression levels of various synaptic genes were analyzed by qRT-PCR in the cortex, hippocampus and cerebellum of WT, HET and KO mice. Statistically significant p values are marked in bold; one-way ANOVA and post-hoc Dunnett's test *vs* WT. Samples were run in triplicates from N = 3 mice per genotype.

Cortex					HIPPOCAMPUS				CEREBELLUM			
	WT	HET	KO		WT	HET	KO		WT	HET	KO	
Target	Mean ± SEM			p	Mean ± SEM			p	Mean ± SEM			p
VGAT	1.07725 ± 0.5607	1.02489 ± 0.3176	0.4711 ± 0.1056	0.4946	0.84369 ± 0.2245	0.72294 ± 0.1203	0.96624 ± 0.3696	0.8085	1.7699 ± 0.9501	1.37634 ± 0.3139	1.34386 ± 0.1461	0.8516
VGLUT1	1.55544 ± 0.2123	1.17194 ± 0.5318	0.83997 ± 0.2249	0.4169	2.58483 ± 0.2881	1.90236 ± 0.9102	1.12895 ± 0.2065	0.2654	0.78733 ± 0.1055	0.35149 ± 0.0678	0.45422 ± 0.1094	**0.0422**
STX1	1.1155 ± 0.6495	1.44595 ± 0.3780	1.13649 ± 0.0877	0.8401	0.3803 ± 0.1671	0.43035 ± 0.0613	0.27751 ± 0.0969	0.6613	0.19563 ± 0.1360	0.04187 ± 0.0106	0.0338 ± 0.0056	0.331
VAMP2	1.81482 ± 0.2717	1.72802 ± 0.2941	1.02679 ± 0.0267	0.0994	1.19396 ± 0.1651	0.78371 ± 0.0379	0.54184 ± 0.0170	**0.0093**	0.92609 ± 0.1989	0.58911 ± 0.0370	0.53118 ± 0.0612	0.1219
SNAP25	1.92039 ± 0.2824	0.83024 ± 0.0914	1.03483 ± 0.0606	**0.0099**	1.43027 ± 0.0905	0.65803 ± 0.0061	0.94071 ± 0.0358	**0.0002**	2.6002 ± 0.5497	1.24115 ± 0.0580	0.97973 ± 0.1044	**0.0256**
SYT1	2.07851 ± 0.2817	0.78103 ± 0.1097	1.04724 ± 0.1269	**0.0065**	1.65559 ± 0.4645	0.90711 ± 0.2018	0.90048 ± 0.1850	0.2235	0.93739 ± 0.3126	0.27308 ± 0.0660	0.36024 ± 0.1117	0.1024
SYT2	0.39727 ± 0.0250	0.18132 ± 0.0415	0.23715 ± 0.0603	**0.0337**	0.44586 ± 0.0856	0.18608 ± 0.0153	0.53445 ± 0.3750	0.5492	5.09159 ± 0.2508	1.12013 ± 0.4215	1.50265 ± 0.1140	**0.0001**
SYP1	1.18741 ± 0.3823	1.57751 ± 0.4001	1.04865 ± 0.0493	0.52	1.75431 ± 0.0805	1.53979 ± 0.0716	0.64376 ± 0.2388	**0.0045**	1.33963 ± 0.7948	0.92669 ± 0.1373	0.6937 ± 0.1701	0.6449
GRIA1	1.04041 ± 0.3712	0.76973 ± 0.2923	0.68713 ± 0.0710	0.6583	0.93965 ± 0.2349	0.66029 ± 0.2700	1.16982 ± 0.1293	0.3285	1.71217 ± 0.5011	1.42481 ± 0.1161	1.55508 ± 0.0429	0.7989

animals in the center *versus* the perimeter of the open field and the frequency of line crossing in these areas were analyzed, suggesting a normal anxiety level in the PRRT2 KO mouse line (Fig. S3D–E). Given the presence of balance problems and backward locomotion in the PRRT2 mouse line, we challenged the motor adaptation/coordination by means of the accelerating Rotarod and foot print tests. In both tests no significant differences between genotypes were found (Fig. S4). Overall our results in the adult PRRT2 KO mice are consistent with the data collected in mouse pups and indicate that the occurrence of paroxysmal events is the main phenotypic trait, in the presence of a normal motor/coordination profile.

3.3.3. Cognitive behavior in PRRT2 adult mice

Since patients bearing homozygous mutations in PRRT2 show a severe encephalopathy associated with intellectual disability, we undertook the study of cognitive behavior in the PRRT2 mouse line using the novel object and cued/contextual fear conditioning tests. Both tests revealed the absence of genotype-specific differences between WT, HET and KO mice. (Figs. S5 and S6). These data suggest that, at least for short-lasting memory, PRRT2 HET and KO mice are not significantly impaired and their performances are indistinguishable from WT littermates.

3.4. Paroxysmal phenotypes of PRRT2 KO mice

Adult PRRT2 KO mice, studied by video-EEG under basal conditions, did not display spontaneous motor seizures or any significant paroxysmal alteration of the major EEG rhythms. However, when PRRT2 KO mice were challenged with a single 60-s 120 dB white tone or with increasing doses of PTZ, they exhibited a strong propensity for the expression of paroxysmal motor behaviors (Fig. 5A).

Virtually 100% of the PRRT2 KO mice presented sound-induced audiogenic seizures (AGS), consisting in a wild, explosive and uncontrolled running episodes that manifested with an average latency of 25.2 ± 7.2 s and an average duration of 18.5 ± 5.4 s. Wild running was mostly unidirectional and was intermingled by back walking episodes that were accompanied by jumping in 50% of the cases (Fig. 5A; Movies S2, S3). However, wild running was never followed by the development of myoclonies or overt tonic-clonic seizures and was characterized by an unaltered cortical EEG (Fig. 5A). Sharply, none of the WT littermates responded to the same sound stimulus with any locomotor activation or epileptic seizure.

The hyperexcitability of brain networks of PRRT2 KO mice was also assessed by the administration of increasing doses of the convulsant PTZ. No significant differences were noticed in the distance travelled or in the duration of the rigidity/freezing episodes at sub-threshold PTZ concentrations, as well as in the threshold for seizures (WT: 57.14 ± 4.21; KO: 58.33 ± 4.77 mg/kg) and in the latency for seizures (WT: 393.2 ± 71.3; KO: 304.3 ± 79.1 s). However, a highly significant longer duration of seizures was observed in PRRT2 KO mice as compared to WT littermates (WT: 28.0 ± 3.3; KO: 151.0 ± 40.7 s; Fig. 5B). When a compound parameter indicating the overall seizure propensity, and including threshold, latency and duration of seizures, was computed (see Materials and Methods), PRRT2 KO mice displayed significantly higher values than their WT companions (WT: 0.20 ± 0.03; KO: 1.20 ± 0.3; Fig. 5B).

3.5. Synaptic connectivity in PRRT2 KO mice

Given that the electrical activity in paroxysmal manifestations is often associated with excitation/inhibition imbalance and/or network instability, we analyzed the number of excitatory and inhibitory synapses (identified as VGLUT1- and VGAT-positive puncta, respectively) in the molecular layer and hilus of DG and in the granular and molecular layers of the cerebellum, two areas where the β-gal staining was most intense.

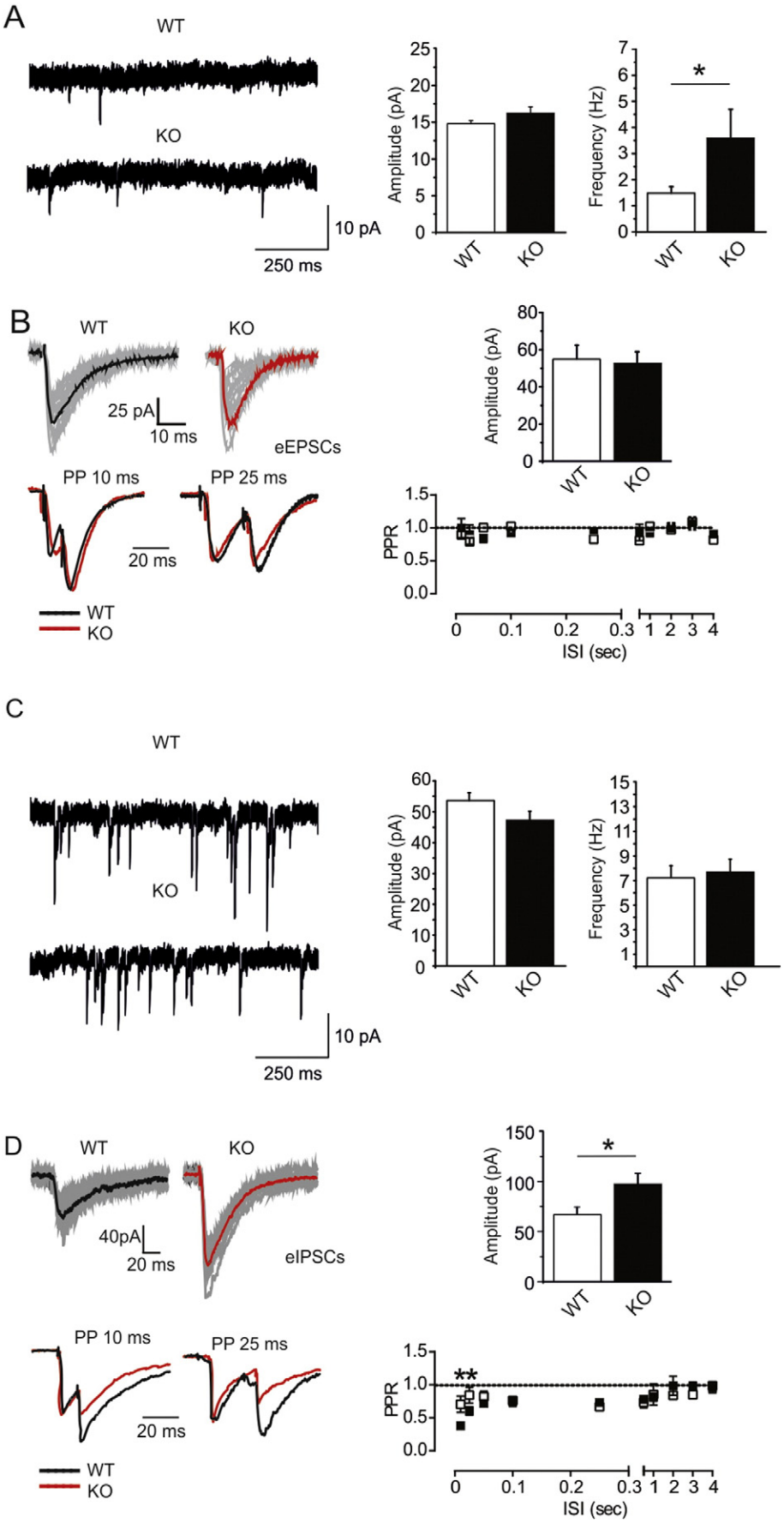
A
WT
KO
10 pA
250 ms
Amplitude (pA)
Frequency (Hz)
*
WT
KO
B
WT
KO
25 pA
10 ms
eEPSCs
PP 10 ms
PP 25 ms
20 ms
WT
KO
Amplitude (pA)
PPR
ISI (sec)
C
WT
KO
10 pA
250 ms
Amplitude (pA)
Frequency (Hz)
D
WT
KO
40pA
20 ms
eIPSCs
PP 10 ms
PP 25 ms
20 ms
WT
KO
Amplitude (pA)
*
PPR
**
ISI (sec)

Analysis of the hilus of DG of PRRT2 KO slices (Fig. 6A) revealed an increase in both VGLUT1 mean intensity (WT: 17.62 ± 0.10; KO: 23.97 ± 1.49; $p < 0.05$) and number of puncta (WT: 1024 ± 95; KO: 2104 ± 106; $p < 0.01$), in the absence of significant differences in VGAT mean intensity or number of puncta. No genotype-dependent changes were observed in the mean intensity and number of puncta of both VGLUT1 and VGAT in the molecular layer of the DG (Fig. S7).

In the granule cell (GC) layer of the cerebellum (Fig. 6B, upper panels), VGAT mean intensity and number of puncta were unchanged, while the VGLUT1 mean intensity, but not the number of puncta, was significantly decreased in PRRT2 KO slices (WT: 11.77 ± 1.37; KO: 4.22 ± 1.14; $p < 0.05$). On the other hand, in the molecular layer of the cerebellum (Fig. 6B, lower panels), an increase in VGAT mean intensity (WT: 22.43 ± 2.83; KO: 54.147 ± 7.859; $p < 0.05$), but not in the number of puncta was observed in PRRT2 KO slices, in the absence of any change in VGLUT1 mean intensity and positive puncta.

We also analyzed the expression levels of synaptic proteins in brain samples from WT, HET and KO mice using qRT-PCR. The analysis was extended to specific synaptic markers, such as synaptophysin1 (SYP1), VGLUT1 and VGAT, as well as to proteins that were previously shown to interact with PRRT2 such as SNAP25, syntaxin1 (STX1), VAMP/synaptobrevin2 (VAMP2), synaptotagmins 1/2 (SYT1/2) and the GRIA1 subunit of AMPA receptors (Lee et al., 2012; Li et al., 2015; Valente et al., 2016). Quantitative analysis of the mRNA levels in the cortex, hippocampus and cerebellum (Table 1) revealed area- and genotype-specific changes in several of the analyzed transcripts. In particular, significant decreases in the mRNAs of SNAP25 and SYT1/2 were observed in the cortex, of SNAP25, VAMP2 and SYP1 in the hippocampus and of SNAP25 and SYT2 in the cerebellum. Notably, most of the transcriptional changes regarded presynaptic PRRT2 interactors, while the expression of its postsynaptic interactor GRIA1 was not affected in any of the three brain areas. In addition, in the cerebellum, a significant decrease in VGLUT1 transcript was observed, consistent with the decreased immunoreactive levels observed with immunohistochemistry.

3.6. Electrophysiology of PRRT2 KO hippocampal and cerebellar slices

To investigate the synaptic effects of PRRT2 deletion in the DG, we made whole-cell voltage-clamp recordings of the DG GCs in hippocampal slices of 4-weeks old PRRT2 KO mice and age-matched WT littermates. We first recorded miniature EPSCs (mEPSCs) from granule neurons in the presence of 0.3 μM tetrodotoxin (TTX). We noticed an over two-fold increase in the frequency of mEPSCs in PRRT2 KO neurons (Fig. 7A), in the absence of any effect on amplitude. We then employed extracellular stimulation of the medial perforant path with paired stimuli to elicit monosynaptic excitatory and inhibitory responses in GCs. No changes between genotypes were observed in the eEPSC amplitude and in the paired pulse ratio at inter-pulse intervals ranging from 10 ms to 4 s (Fig. 7B). When inhibitory transmission was analyzed, no significant changes in either frequency or amplitude of miniature IPSCs (mIPSCs) were noticed (Fig. 7C). However, when evoked inhibitory monosynaptic responses were analyzed, the amplitude of eIPSCs was significantly increased in PRRT2 KO neurons with a corresponding significant decrease in the PPR at short inter-pulse intervals (ISI: 10–25 ms) (Fig. 7D). No significant changes in the dynamics of depression during high frequency trains (2 s @ 40 Hz) were observed in PRRT2 KO mice for both excitatory and inhibitory transmission (Fig. S8).

Given the high PRRT2 expression in cerebellar granule cells, and the motor phenotype of PRRT2 KO mice, we next concentrated on the analysis of the PF-PC synapse. Purkinje cells in sagittal cerebellar slices obtained from juvenile (4-weeks old) WT and PRRT2 KO littermates were patched in the presence of a complete blockade of NMDA, $GABA_A$, pre- and post-synaptic $GABA_B$, CB1 and mGLU1 receptors to limit modulation of EPSC amplitude by stimulation-dependent activation of these receptors. No significant changes were observed in the frequency and amplitude of mEPSCs recorded in the presence of TTX (Fig. 8A). The absence of postsynaptic effects and the unchanged frequency of mEPSCs are consistent with the absence of PRRT2 expression in PCs and with a normal density of VGLUT1 puncta labeling the PF terminals in the molecular layer (Figs. 3E and 6B). When postsynaptic responses were evoked by minimal extracellular stimulation of parallel fibers in the molecular layer with single and paired stimuli at increasing ISIs (from 10 ms to 4 s), no changes were observed in both eEPSC amplitude and PPR at any of the intervals tested (Fig. 8B). Next, we subjected the PF/PC synapse to high frequency stimulation trains at various frequencies from 10 to 40 Hz lasting 2 s (Fig. 8C) to assess the presynaptic dynamics of short-term plasticity and the rate of replenishment of the release sites in the presence or absence of PRRT2. Under the experimental conditions used, synaptic responses in WT slices exhibited an early facilitation phase followed by a depression phase, the amplitude of which were both proportional to the stimulation frequency. Strikingly, in PRRT2 KO synapses facilitation was long lasting and depression was not present even at the highest stimulations frequency. The effect was particularly evident when cumulative plots of EPSC amplitude, normalized by the first response in the train, were extracted from the data. In PRRT2 KO synapses, significantly higher slopes were present at all tested frequencies, indicating an accelerated replenishment of the readily releasable pool.

4. Discussion

As PRRT2 mutations are predominantly loss-of-function, the PRRT2 KO mouse described here represents an important experimental model to reproduce the conditions of PRRT2 deficiency present in the patients.

4.1. PRRT2 has a very specific regional expression in the central nervous system

PRRT2 has a strictly area-specific expression, as deduced from β-gal expression driven by the PRRT2 promoter. β-gal was expressed in characteristic regions of the central nervous system (CNS), but was not widespread. Interestingly, the expression was particularly high in neurons of the lower hindbrain, cerebellum and spinal cord, reminiscent of the expression pattern of its major interactor Syt2 (Pang et al., 2006; Valente et al., 2016). While a substantial agreement exists with the levels of the PRRT2 protein for cerebellum and hippocampus, a discrepancy was observed in the basal ganglia and neocortex that exhibit low mRNA levels and high levels of the PRRT2 protein. Taking into account the predominant presynaptic expression of PRRT2, this means that neocortex and basal ganglia are targets of projections coming from other areas rich in PRRT2-expressing neurons.

Some specific sites of high PRRT2 mRNA expression are noteworthy. Areas of very high expression include the claustrum, some thalamic

Fig. 7. Electrophysiology of PRRT2 KO hippocampal slices. A. Representative mEPSC traces recorded in DG GCs from WT and PRRT2 KO mice in the presence of TTX. The mean (±SEM) amplitude and frequency of mEPSCs are reported on the right for WT (open bars) and PRRT2 KO (black bars) mice. *$p < 0.05$, two-tailed unpaired Student's *t*-test. N = 18 and 12 neurons from WT (3 mice) and PRRT2 KO (3 mice), respectively. B. *Left:* Representative traces of eEPSCs from WT (black traces) and KO (red traces) DG GCs in response to single (top) or paired (bottom) stimuli. *Right:* Mean (±SEM) eEPSC amplitude (top) and paired-pulse ratio (PPR) plotted as a function of the inter-stimulus interval (ISI: 10 ms-4 s) for WT (open bar/symbol) and PRRT2 KO (black bar/symbol) mice. N = 14 and 13 neurons from WT (4 mice) and PRRT2 KO (4 mice), respectively. C. Representative mIPSC traces recorded in GCs from WT and PRRT2 KO mice in the presence of TTX. The mean (±SEM) amplitude and frequency of mIPSCs are reported on the right for WT (open bars) and PRRT2 KO (black bars) mice. N = 20 and 17 neurons from WT (3 mice) and PRRT2 KO (3 mice), respectively. D. *Left:* Representative traces of eIPSCs from WT (black traces) and KO (red traces) DG GCs in response to single (top) or paired (bottom) stimuli. *Right:* Mean (±SEM) eIPSC amplitude (top) and paired-pulse ratio (PPR) plotted as a function of the ISI (10 ms-4 s) for WT (open bar/symbol) and PRRT2 KO (black bar/symbol) mice. *$p < 0.05$, two-tailed unpaired Student's *t*-test. N = 13 and 12 neurons from WT (4 mice) and PRRT2 KO (4 mice), respectively.

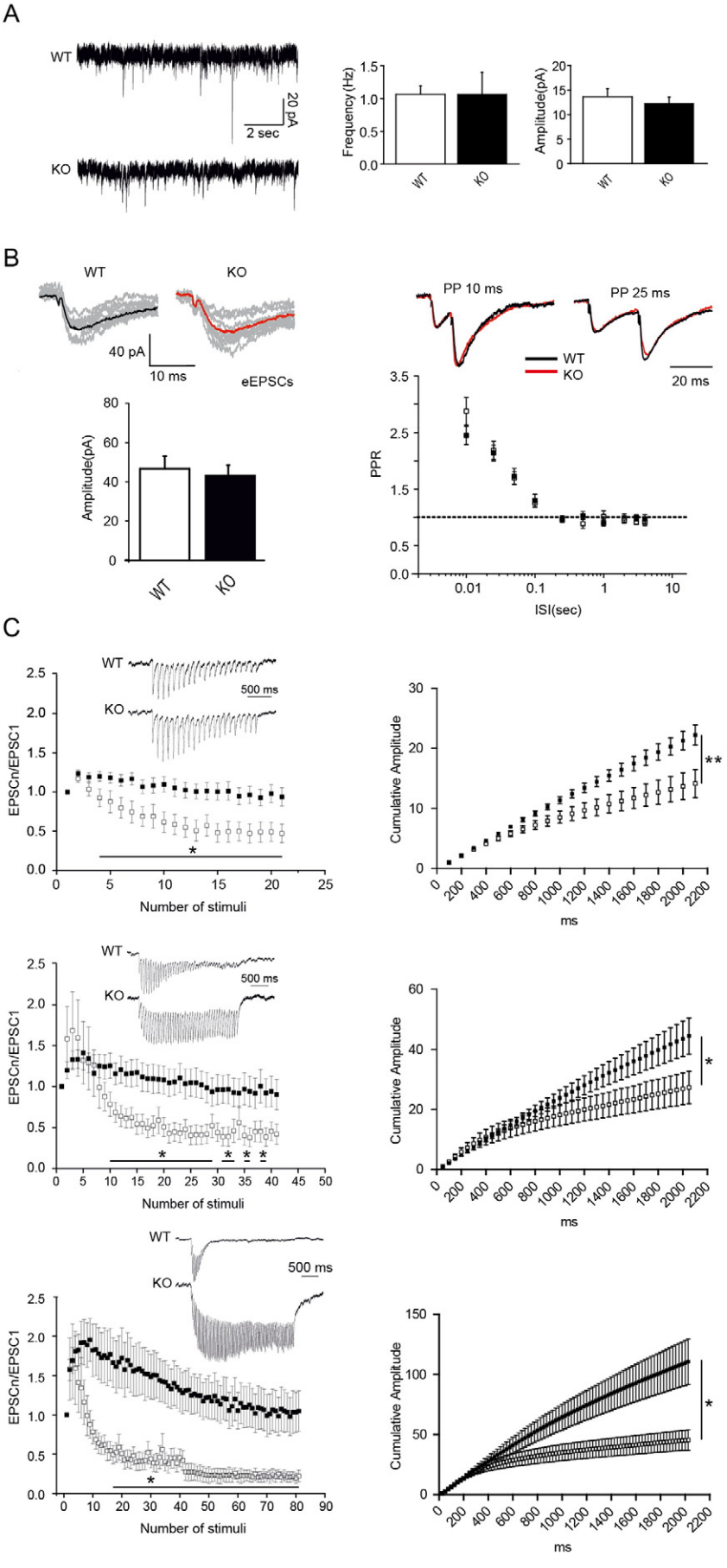
A
WT
KO
20 pA
2 sec
Frequency (Hz)
Amplitude(pA)
B
WT
KO
40 pA
10 ms
eEPSCs
Amplitude(pA)
PP 10 ms
PP 25 ms
20 ms
PPR
ISI(sec)
C
EPSCn/EPSC1
500 ms
Number of stimuli
Cumulative Amplitude
ms

nuclei, amygdala, tectum and the dorsal horn of the spinal cord, all areas involved in processing sensory information. The intense staining of the dorsal horn of the spinal cord, and in particular of the *substantia gelatinosa*, in which physiological processing of somatosensory and nociceptive stimuli takes place (Zeilhofer et al., 2012), also implicates PRRT2 in the relay between sensory information and motor output.

The only strongly labeled neocortical layer VIb projects specifically to the claustrum (Goll et al., 2015). On the other hand, the claustro-cortical connectivity is mediated by strong glutamatergic projections to many cortical layers, primarily layer IV, but also layers I/II and VI. The abundant glutamatergic claustro-cortical connections, together with the presynaptic targeting of the PRRT2 protein can account for the high PRRT2 immunoreactivity present in the cortex. The high PRRT2 expression occurring in claustrum and layer VIb of the cortex suggests an involvement of PRRT2 in the cortical/claustral/cortical circuit that plays an important role in multi-sensory integration and sensorimotor coordination and can be potentially involved in the pathogenesis of sensory-triggered paroxysmal events (Goll et al., 2015; Italiano et al., 2016).

In the hippocampus, positivity is concentrated in the hilus of DG, where mossy cells are present and control the excitability of DG GCs. Glutamatergic mossy cells have a mild excitatory effect on GCs, but that also activate DG interneurons that potently inhibit GCs. Because of this feed-forward inhibition, mossy cells are believed to prevent seizures and their impairment has been often associated with epilepsy of hippocampal origin (Scharfman, 2016; Toader et al., 2013).

4.2. PRRT2 KO mice do not have overt abnormalities in brain development

PRRT2 inactivation did not affect the viability of the KO embryos or their survival after birth. The absence of peripheral pathologies is consistent with the neuron-specific expression of PRRT2 (Chen et al., 2011; Lee et al., 2012; Valente et al., 2016), while the absence of an overt neurological phenotype indicates that PRRT2 is dispensable for basal CNS functions.

Paroxysmal disorders, such as partial epilepsies, often result from brain lesions or dysplasia. Despite no major abnormalities were observed in the brain morphology of PRRT2 KO mice, a detailed analysis of the architecture of the neocortex, hippocampus and cerebellum revealed a consistently decreased neocortical thickness in sensory areas (*e.g.* the somatosensory and visual cortices), with no detectable changes in hippocampus, cerebellum or white matter cytoarchitecture. This finding is consistent with the delayed migration of cortical neurons during development and the decreased synaptic density observed *in vitro* and *in vivo* upon downregulation of PRRT2 expression (Liu et al., 2016; Valente et al., 2016).

4.3. PRRT2 KO mice display motor paroxysms

Both pups and adult KO mice were not affected by spontaneous seizures and their intercritical EEG did not exhibit any abnormalities, indicating a normal basal rhythmogenesis. However, they displayed a sharp paroxysmal phenotype, including gait problems and paroxysmal back walking, that recapitulates the most common clinical manifestations of the human PRRT2-linked diseases. These episodes were present from the early stages of life and were also detectable in the adult, reminiscent of the early temporal window of the pathologic manifestations in patients (Ebrahimi-Fakhari et al., 2015). These disturbances are reminiscent of episodic ataxia found in patients bearing PRRT2 mutations and strongly implicate the cerebellum, a brain region with very high PRRT2 expression, in their pathogenesis.

PRRT2 KO mice were highly prone to audiogenic paroxysms with wild running, back walking and jumping and displayed a higher propensity for generalized PTZ-evoked seizures. In both kinds of provocations, however, the seizure propensity was not very severe, consistent with the mild epileptic phenotype of patients bearing PRRT2 mutations (Ebrahimi-Fakhari et al., 2015; Gardiner et al., 2015; Heron and Dibbens, 2013). In fact, AGS never progressed beyond the wild running stage and the convulsive threshold for PTZ in PRRT2 KO mice was similar to WT animals, although tonic seizures were more severe. The epileptic nature of wild running in response to audiogenic stimuli has been supported by its potential progression to generalized seizures (Simler and Vergnes, 1999; Vinogradova, 2015). It is known that high sensitivity to AGS involves neuronal networks located primarily in the brainstem, including the inferior and superior colliculi and the periaqueductal grey (Chakravarty and Faingold, 1999; Faingold, 1999; N'Gouemo and Faingold, 1999). The amygdala complex is also involved in the generation of AGS, although its role becomes primary in AGS kindling (Chakravarty and Faingold, 1999). Notably, high expression levels of β-gal/PRRT2 are present in the colliculi, periaqueductal grey and amygdala. However, the lack of progression to tonic-clonic seizures, the preserved EEGgraphic activity and consciousness, together with the presence of back walking make these episodes resemble paroxysmal compulsive motor manifestations of complex nature, in which dysfunctions of multiple brain circuits, including the cerebellum, may be involved.

The vast majority of patients carry PRRT2 mutations in heterozygosity (Heron and Dibbens, 2013). However, heterozygous mice do not display any pathogenic phenotype, except for the persistence of bouncing during postnatal development. In contrast, the few patients described with homozygous or compound mutations display a severe phenotype characterized by combination of multiple paroxysmal neurological disorders, severity and persistence of the paroxysmal attacks, occurrence of unusually prolonged ataxia episodes, presence of intractable epilepsy associated with sign of encephalopathy (Delcourt et al., 2015; Labate et al., 2012). The motor/epileptic phenotype of homozygous PRRT2 KO mice in response to environmental stimuli is reminiscent of the severe manifestations experienced by homozygous patients, although no spontaneous seizures or marked cognitive impairments were observed.

4.4. How are PRRT2-linked motor paroxysms generated?

Acute silencing of PRRT2 in wild type neurons induced a sharp decrease of evoked synchronous transmission due to the loss of Ca^{2+} sensitivity of the release process. The substantial absence of gross behavioral alterations under basal conditions suggests that compensatory mechanisms during development might have come into play. However, the transition between the basal state and paroxysmal activity implies that the chronic absence of PRRT2 induces functional abnormalities in specific networks due to developmental defects or network instability.

PRRT2 KO mice displayed a specifically altered plasticity at the PF-PC synapses of the cerebellum, in the absence of major changes in basal

Fig. 8. Electrophysiology of PRRT2 KO cerebellar slices. A. Representative mEPSC traces recorded in PCs from WT and PRRT2 KO mice in the presence of TTX. The mean (±SEM) amplitude and frequency of mEPSCs are reported on the right for WT (open bars) and PRRT2 KO (black bars) mice. N = 9 and 11 neurons from WT (3 mice) and PRRT2 KO (3 mice), respectively. B. *Left:* Representative traces of eEPSCs from WT (black traces) and KO (red traces) mice in response to single (top) or paired (bottom) stimuli. *Right:* Mean (±SEM) eEPSC amplitude (top) and paired-pulse ratio (PPR) plotted as a function of the inter-stimulus interval (ISI: 10 ms-4 s) for WT (open bar/symbol) and PRRT2 KO (black bar/symbol) mice. C. PRRT2 knockdown enhances synaptic facilitation during high frequency trains. *Left:* Mean (±SEM) normalized values of eEPSC amplitude showing the time course of synaptic facilitation and depression in PCs subjected to 2 s high-frequency stimulation at 10 (top), 20 (middle) and 40 (bottom) Hz. In the insets, representative traces showing synchronous EPSCs evoked by the tetanic stimulation. *Right:* Cumulative plots of normalized EPSC amplitudes during trains at 10 (top), 20 (middle) and 40 (bottom) Hz plotted as means (±SEM) against the stimulus number. Individual slopes were calculated from the last 10 responses in the train and statistically compared (10 Hz: 0.006 ± 0.001 and 0.010 ± 0.001, $p < 0.01$; 20 Hz: 0.011 ± 0.002 and 0.021 ± 0.003, $p < 0.05$; 40 Hz: 0.017 ± 0.004 and 0.054 ± 0.010, $p < 0.05$; for WT and PRRT2 KO neurons, respectively). *$p < 0.05$; **$p < 0.01$, two-tailed unpaired Student's *t*-test. N = 11 and 18 neurons from WT (3 mice) and PRRT2 KO (3 mice), respectively.

transmission. This phenotype may alter the properties of the high-frequency transmission between granule cells, expressing very high PRRT2 levels, and the PC output of the cerebellar cortex. Indeed, ataxia and motor coordination problems can result from dysfunctions in short- and long-term plasticity properties at the PF-PC synapse, in which the fine-tuning of sensorimotor information in response to changing behavioral needs is altered (Becker, 2014).

Synaptic transmission in the DG of the hippocampus was also investigated as DG is one of the forebrain areas with the highest PRRT2 expression and is known to filter sensory information entering the hippocampus from the cortex. However, synaptic transmission in the DG was not markedly altered except for an increased frequency of mEPSCs, mirrored by an increased density of VGLUT1-positive synapses, and a likely compensatory increase in the strength of evoked GABAergic transmission.

4.5. Are there shared mechanisms for motor paroxysms?

Recurrent neurological dysfunctions present in several disorders including epilepsy, episodic ataxia and hemiplegic migraine are thought to involve similar pathogenetic mechanisms in which a trigger induces an attack in subjects that are otherwise normal. Mutations in PRRT2, PNKD, P/Q-type Ca^{2+} (Cav2.1) and TRPC3 channels have all been associated with a variety of paroxysmal disorders in man and mouse, such as kinesigenic dyskinesia and/or coreoathetosis (Ebrahimi-Fakhari et al., 2015), non-kinesigenic dyskinesia (Shen et al., 2015), *tottering* or *lethargic*-type of dyskinesia (Khan and Jinnah, 2002; Matsushita et al., 2002) and *moonwalker*-type of cerebellar ataxia (Becker et al., 2009). The ataxic PNKD KO mouse is particularly interesting, as it involves the mutation of a presynaptic protein interacting with RIM1 that, similarly to PRRT2, is highly expressed in the cerebellum and participates in the post-docking steps of exocytosis (Shen et al., 2015).

From a behavioral standpoint, the paroxysmal dyskinesia *tottering*, *lethargic and moonwalker* models share similar aspects with the PRRT2 KO mouse. *Tottering* mice exhibit stereotyped attacks of dystonia triggered by stress, caffeine or ethanol (Raike et al., 2013) and bear mutations in Cav2.1 (P/Q-type) that in human are associated with episodic ataxia and hemiplegic migraine, two pathologies also linked to PRRT2 mutations. *Lethargic* mice, bearing mutations in the Cav2.1 β4 auxiliary subunit, also display absence epilepsy and attacks of motor disability. Finally, *moonwalker* mice, exhibiting the most similar phenotype to PRRT2 KO mice, with backward locomotion and motor coordination deficits, bear a mutation in the non-selective cation channel TRPC3 that, similarly to PRRT2, is highly expressed in the cerebellum (Becker, 2014; Becker et al., 2009).

When the causative genes of paroxysmal motor dysfunctions in these mouse models are considered, two functional groups of affected genes emerge: (i) one group of Ca^{2+} channels; (ii) another group of presynaptic proteins (PRRT2, PNKD) involved in interactions with presynaptic Ca^{2+} channels or regulating the Ca^{2+} sensitivity of exocytosis (Shen et al., 2015; Valente et al., 2016). Although the former disorders can be considered channelopathies and the latter synaptopathies, it is possible that in both cases presynaptic Ca^{2+} signaling and Ca^{2+}-dependent neurotransmitter release are severely disturbed, leading to network instability/hyperexcitability and thereby to paroxysmal disorders.

In conclusion, this study describes for the first time the phenotype of KO mice for PRRT2 and shows that its loss-of-function recapitulates the human phenotype in terms of episodic disturbances in motor coordination and paroxysmal dyskinesias, suggesting that PRRT2 plays a critical role in the development of cortical connectivity and functional stability of neuronal networks. From these considerations, the PRRT2 KO mouse emerges as a promising experimental model and as a starting point to identify therapeutic targets and refine specific drug approaches of PRRT2-related diseases.

Supplementary data to this article can be found online at http://dx.doi.org/10.1016/j.nbd.2016.12.018.

Funding

The work was supported by research grants from Telethon-Italy (grant number GGP13033 to FB, FV and FZ); Compagnia di San Paolo (grant number 2015-0546 to FB); European Union FP7 Integrating Project “Desire” (grant number 602531 to FB and FZ); European Union “ECMED” (grant number 642881 to FB); CARIPLO Foundation (grant number 2013-0879 to FV and FB); and Italian Ministry of Health Ricerca Finalizzata (grant number RF-2011-02348476 to FV, FB and FZ).

Conflict of interest statement

The authors declare no competing financial interests.

Acknowledgements

We thank the IMPC European Consortium at the Sanger Institute (UK) in the frame of the European EMMA/Infrafrontier for making available the PRRT2 KO mouse (Allele:$Prrt2^{tm1a\ (KOMP)Wtsi}$). We thank Drs. Elodie Chabrol (Institute of Neurology, University College London, UK) for help in setting up the wireless EEG system, Andrea Contestabile (Italian Institute of Technology, Genova, Italy) for advice and supply of PTZ, Frederic Doussau (CNRS Strasbourg, France) for advice for the experiments in cerebellar slices, Monica Morini (Italian Institute of Technology, Genova, Italy) and Michele Cilli (IRCCS San Martino, Genova, Italy) for help in breeding the mice, Diego Moruzzo (Center for Synaptic Neuroscience, Istituto Italiano di Tecnologia, Genova, Italy) for assistance in genotyping assays.

References

Becker, E.B.E., 2014. The Moonwalker mouse: new insights into TRPC3 function, cerebellar development, and ataxia. Cerebellum http://dx.doi.org/10.1007/s12311-014-0564-5.

Becker, E.B.E., Oliver, P.L., Glitsch, M.D., Banks, G.T., Achilli, F., Hardy, A., Nolan, P.M., Fisher, E.M.C., Davies, K.E., 2009. A point mutation in TRPC3 causes abnormal Purkinje cell development and cerebellar ataxia in moonwalker mice. Proc. Natl. Acad. Sci. U. S. A. 106:6706–6711. http://dx.doi.org/10.1073/pnas.0810599106.

Boyken, J., Grønborg, M., Riedel, D., Urlaub, H., Jahn, R., Chua, J., 2013. Molecular profiling of synaptic vesicle docking sites reveals novel proteins but few differences between glutamatergic and GABAergic synapses. Neuron 78:285–297. http://dx.doi.org/10.1016/j.neuron.2013.02.027.

Browning, R.A., Nelson, D.K., 1986. Modification of electroshock and pentylenetetrazol seizure patterns in rats affer precollicular transections. Exp. Neurol. 93:546–556. http://dx.doi.org/10.1016/0014-4886(86)90174-3.

Capoccia, S., Maccarinelli, F., Buffoli, B., Rodella, L.F., Cremona, O., Arosio, P., Cirulli, F., 2015. NBehavioral Characterization of Mouse Models of Neuroferritinopathyo Title. PLoS One 10. http://dx.doi.org/10.1371/journal.pone.0118990.

Chakravarty, D.N., Faingold, C.L., 1999. Differential roles in the neuronal network for audiogenic seizures are observed among the inferior colliculus subnuclei and the amygdala. Exp. Neurol. 157:135–141. http://dx.doi.org/10.1006/exnr.1999.7047.

Chang, P., Hashemi, K.S., Walker, M.C., 2011. A novel telemetry system for recording EEG in small animals. J. Neurosci. Methods 201:106–115. http://dx.doi.org/10.1016/j.jneumeth.2011.07.018.

Chen, W.-J., Lin, Y., Xiong, Z.-Q., Wei, W., Ni, W., Tan, G.-H., Guo, S.-L., He, J., Chen, Y.-F., Zhang, Q.-J., Li, H.-F., Lin, Y., Murong, S.-X., Xu, J., Wang, N., Wu, Z.-Y., 2011. Exome sequencing identifies truncating mutations in PRRT2 that cause paroxysmal kinesigenic dyskinesia. Nat. Genet. 43:1252–1255. http://dx.doi.org/10.1038/ng.1008.

De Filippis, B., Ricceri, L., Laviola, G., 2010. Early postnatal behavioral changes in the Mecp2-308 truncation mouse model of Rett syndrome. Genes. Brain Behav. 9:213–223. http://dx.doi.org/10.1111/j.1601-183X.2009.00551.x.

Deidda, G., Parrini, M., Naskar, S., Bozarth, I.F., Contestabile, A., Cancedda, L., 2015. Reversing excitatory GABAAR signaling restores synaptic plasticity and memory in a mouse model of Down syndrome. Nat. Med. 21:318–326. http://dx.doi.org/10.1038/nm.3827.

Delcourt, M., Riant, F., Mancini, J., Milh, M., Navarro, V., Roze, E., Humbertclaude, V., Korff, C., Des Portes, V., Szepetowski, P., Doummar, D., Echenne, B., Quintin, S., Leboucq, N., Singh Amrathlal, R., Rochette, J., Roubertie, A., 2015. Severe phenotypic spectrum of biallelic mutations in PRRT2 gene. J. Neurol. Neurosurg. Psychiatry 86:782–785. http://dx.doi.org/10.1136/jnnp-2014-309025.

Ebrahimi-Fakhari, D., Saffari, A., Westenberger, A., Klein, C., 2015. The evolving spectrum of PRRT2-associated paroxysmal diseases. Brain 138:3476–3495. http://dx.doi.org/10.1093/brain/awv317.

Faingold, C.L., 1999. Neuronal networks in the genetically epilepsy-prone rat. Adv. Neurol. 79, 311–321.

Gardiner, A.R., Jaffer, F., Dale, R.C., Labrum, R., Erro, R., Meyer, E., Xiromerisiou, G., Stamelou, M., Walker, M., Kullmann, D., Warner, T., Jarman, P., Hanna, M., Kurian,

M.A., Bhatia, K.P., Houlden, H., 2015. The clinical and genetic heterogeneity of paroxysmal dyskinesias. Brain 138:3567–3580. http://dx.doi.org/10.1093/brain/awv310.
Gazzerro, E., Baldassari, S., Giacomini, C., Musante, V., Fruscione, F., la Padula, V., Biancheri, R., Scarfì, S., Prada, V., Sotgia, F., Duncan, I.D., Zara, F., Werner, H.B., Lisanti, M.P., Nobbio, L., Corradi, A., Minetti, C., 2012. Hyccin, the molecule mutated in the leukodystrophy hypomyelination and congenital cataract (HCC), is a neuronal protein. PLoS One 7. http://dx.doi.org/10.1371/journal.pone.0032180.
Goll, Y., Atlan, G., Citri, A., 2015. Attention: the claustrum. Trends Neurosci. 38:486–495. http://dx.doi.org/10.1016/j.tins.2015.05.006.
Heron, S.E., Dibbens, L.M., 2013. Role of PRRT2 in common paroxysmal neurological disorders: a gene with remarkable pleiotropy. J. Med. Genet. 50:133–139. http://dx.doi.org/10.1136/jmedgenet-2012-101406.
Huang, X.-J., Wang, T., Wang, J.-L., Liu, X.-L., Che, X.-Q., Li, J., Mao, X., Zhang, M., Bi, G.-H., Wu, L., Zhang, Y., Wang, J.-Y., Shen, J.-Y., Tang, B.-S., Cao, L., Chen, S.-D., 2015. Paroxysmal kinesigenic dyskinesia: clinical and genetic analyses of 110 patients. Neurology 85:1546. http://dx.doi.org/10.1212/WNL.0000000000002079.
Italiano, D., Striano, P., Russo, E., Leo, A., Spina, E., Zara, F., Striano, S., Gambardella, A., Labate, A., Gasparini, S., Lamberti, M., De Sarro, G., Aguglia, U., Ferlazzo, E., 2016. Genetics of reflex seizures and epilepsies in humans and animals. Epilepsy Res. 121: 47–54. http://dx.doi.org/10.1016/j.eplepsyres.2016.01.010.
Khan, Z., Jinnah, H.a., 2002. Paroxysmal dyskinesias in the lethargic mouse mutant. J. Neurosci 22, 8193–8200 doi:22/18/8193 [pii] ET - 2002/09/12.
Labate, A., Tarantino, P., Viri, M., Mumoli, L., Gagliardi, M., Romeo, A., Zara, F., Annesi, G., Gambardella, A., 2012. Homozygous c.649dupC mutation in PRRT2 worsens the BFIS/PKD phenotype with mental retardation, episodic ataxia, and absences. Epilepsia 53. http://dx.doi.org/10.1111/epi.12009.
Lee, H.Y., Huang, Y., Bruneau, N., Roll, P., Roberson, E.D.O., Hermann, M., Quinn, E., Maas, J., Edwards, R., Ashizawa, T., Baykan, B., Bhatia, K., Bressman, S., Bruno, M.K., Brunt, E.R., Caraballo, R., Echenne, B., Fejerman, N., Frucht, S., Gurnett, C.A., Hirsch, E., Houlden, H., Jankovic, J., Lee, W.L., Lynch, D.R., Mohammed, S., Müller, U., Nespeca, M.P., Renner, D., Rochette, J., Rudolf, G., Saiki, S., Soong, B.W., Swoboda, K.J., Tucker, S., Wood, N., Hanna, M., Bowcock, A.M., Szepetowski, P., Fu, Y.H., Ptáček, L.J., 2012. Mutations in the Gene PRRT2 Cause Paroxysmal Kinesigenic Dyskinesia with Infantile Convulsions. Cell Rep. 1:2–12. http://dx.doi.org/10.1016/j.celrep.2011.11.001.
Li, M., Niu, F., Zhu, X., Wu, X., Shen, N., Peng, X., Liu, Y., 2015. PRRT2 mutant leads to dysfunction of glutamate signaling. Int. J. Mol. Sci. 16:9134–9151. http://dx.doi.org/10.3390/ijms16059134.
Liu, Y.T., Nian, F.S., Chou, W., Tai, C.Y., Kwan, S.Y., Chen, C., Kuo, P.W., Lin, P.H., Chen, C.Y., Huang, C.W., Lee, Y.C., Soong, B.W., T., J., 2016. PRRT2 mutations lead to neuronal dysfunction and neurodevelopmental defects. Oncotarget in press. 10.18632/oncotarget.9258.
Matsushita, K., Wakamori, M., Rhyu, I.J., Arii, T., Oda, S., Mori, Y., Imoto, K., 2002. Bidirectional alterations in cerebellar synaptic transmission of tottering and rolling Ca2 + channel mutant mice. J. Neurosci. 22, 4388–4398 doi:20026451\r22/11/4388 [pii].
McLeod, F., Ganley, R., Williams, L., Selfridge, J., Bird, A., Cobb, S.R., 2013. Reduced seizure threshold and altered network oscillatory properties in a mouse model of Rett syndrome. Neuroscience 231:195–205. http://dx.doi.org/10.1016/j.neuroscience.2012.11.058.
Medrihan, L., Cesca, F., Raimondi, A., Lignani, G., Baldelli, P., Benfenati, F., 2013. Synapsin II desynchronizes neurotransmitter release at inhibitory synapses by interacting with presynaptic calcium channels. Nat. Commun. 4:1512. http://dx.doi.org/10.1038/ncomms2515.
N'Gouemo, P., Faingold, C.L., 1999. The periaqueductal grey is a critical site in the neuronal network for audiogenic seizures: modulation by GABA(A), NMDA and opioid receptors. Epilepsy Res. 35:39–46. http://dx.doi.org/10.1016/S0920-1211(98)00128-4.
Pang, Z.P., Melicoff, E., Padgett, D., Liu, Y., Teich, A.F., Dickey, B.F., Lin, W., Adachi, R., Südhof, T.C., 2006. Synaptotagmin-2 is essential for survival and contributes to Ca2 + triggering of neurotransmitter release in central and neuromuscular synapses. J. Neurosci. 26:13493–13504. http://dx.doi.org/10.1523/JNEUROSCI.3519-06.2006.
Paxinos, G., Franklin, K.B.J., 29 Oct 2012. Imprint: Academic Press, p. 360, ISBN: 9780123910578.
Pfaffl, M.W., 2001. A new mathematical model for relative quantification in real-time RT-PCR. Nucleic Acids Res. 29 (e45). http://dx.doi.org/10.1093/nar/29.9.e45.
Raike, R.S., Weisz, C., Hoebeek, F.E., Terzi, M.C., De Zeeuw, C.I., van den Maagdenberg, A.M., Jinnah, H.A., Hess, E.J., 2013. Stress, caffeine and ethanol trigger transient neurological dysfunction through shared mechanisms in a mouse calcium channelopathy. Neurobiol. Dis. 50:151–159. http://dx.doi.org/10.1016/j.nbd.2012.09.005.
Rantala, J., Kemppainen, S., Ndode-Ekane, X.E., Lahtinen, L., Bolkvadze, T., Gurevicius, K., Tanila, H., Pitkänen, A., 2015. Urokinase-type plasminogen activator deficiency has little effect on seizure susceptibility and acquired epilepsy phenotype but reduces spontaneous exploration in mice. Epilepsy Behav. 42:117–128. http://dx.doi.org/10.1016/j.yebeh.2014.11.001.
Romano, E., Michetti, C., Caruso, A., Laviola, G., Scattoni, M.L., 2013. Characterization of neonatal vocal and motor repertoire of reelin mutant mice. PLoS One 8.
Rossi, P., Sterlini, B., Castroflorio, E., Marte, A., Onofri, F., Valtorta, F., Maragliano, L., Corradi, A., Benfenati, F., 2016. A novel topology of proline-rich transmembrane protein 2 (PRRT2): hints for an intracellular function at the synapse. J. Biol. Chem. 291: 6111–6123. http://dx.doi.org/10.1074/jbc.M115.683888.
Scattoni, M.L., Martire, A., Cartocci, G., Ferrante, A., Ricceri, L., 2013. Reduced social interaction, behavioural flexibility and BDNF signalling in the BTBR T + tf/J strain, a mouse model of autism. Behav. Brain Res. 251:35–40. http://dx.doi.org/10.1016/j.bbr.2012.12.028.
Scharfman, H., 2016. The enigmatic mossy cell of the dentate gyrus. Nat. Rev. Neurosci. 17:562–575. http://dx.doi.org/10.1038/nrn.2016.87.
Scheffer, I.E., Grinton, B.E., Heron, S.E., Kivity, S., Afawi, Z., Iona, X., Goldberg-Stern, H., Kinali, M., Andrews, I., Guerrini, R., Marini, C., Sadleir, L.G., Berkovic, S.F., Dibbens, L.M., 2012. PRRT2 phenotypic spectrum includes sporadic and fever-related infantile seizures. Neurology 79:2104–2108. http://dx.doi.org/10.1212/WNL.0b013e3182752c6c.
Shen, Y., Ge, W.-P., Li, Y., Hirano, A., Lee, H.-Y., Rohlmann, A., Missler, M., Tsien, R.W., Jan, L.Y., Fu, Y.-H., Ptáček, L.J., 2015. Protein mutated in paroxysmal dyskinesia interacts with the active zone protein RIM and suppresses synaptic vesicle exocytosis. Proc. Natl. Acad. Sci. U. S. A. 112:2935–2941. http://dx.doi.org/10.1073/pnas.1501364112.
Simler, S., Vergnes, M., M., C., 1999. Spatial and temporal relationships between C-Fos expression and kindling of audiogenic seizures in Wistar rats. Exp. Neurol. 157, 106–119.
Skarnes, W.C., Rosen, B., West, A.P., Koutsourakis, M., Bushell, W., Iyer, V., Mujica, A.O., Thomas, M., Harrow, J., Cox, T., Jackson, D., Severin, J., Biggs, P., Fu, J., Nefedov, M., de Jong, P.J., Stewart, a.F., Bradley, A., 2011. A conditional knockout resource for the genome-wide study of mouse gene function. Nature 474:337–342. http://dx.doi.org/10.1038/nature10163.
Toader, O., Forte, N., Orlando, M., Ferrea, E., Raimondi, A., Baldelli, P., Benfenati, F., Medrihan, L., 2013. Dentate gyrus network dysfunctions precede the symptomatic phase in a genetic mouse model of seizures. Front. Cell. Neurosci. 7:138. http://dx.doi.org/10.3389/fncel.2013.00138.
Valente, P., Castroflorio, E., Rossi, P., Fadda, M., Sterlini, B., Cervigni, R.I., Prestigio, C., Giovedi, S., Onofri, F., Mura, E., Guarnieri, F.C., Marte, A., Orlando, M., Zara, F., Fassio, A., Valtorta, F., Baldelli, P., Corradi, A., Benfenati, F., 2016. PRRT2 is a key component of the Ca2 + -dependent neurotransmitter release machinery. Cell Rep. 15:117–131. http://dx.doi.org/10.1016/j.celrep.2016.03.005.
Valera, A.M., Doussau, F., Poulain, B., Barbour, B., Isope, P., 2012. Adaptation of granule cell to purkinje cell synapses to high-frequency transmission. J. Neurosci. 32:3267–3280. http://dx.doi.org/10.1523/JNEUROSCI.3175-11.2012.
Valtorta, F., Benfenati, F., Zara, F., Mendolesi, J., 2016. PRRT2: from paroxysmal disorders to regulation of synaptic function. Trends Neurosci. in press.
Vigevano, F., 2005. Benign familial infantile seizures. Brain and Development:pp. 172–177 http://dx.doi.org/10.1016/j.braindev.2003.12.012.
Vinogradova, L.V., 2015. Audiogenic kindling and secondary subcortico-cortical epileptogenesis: Behavioral correlates and electrographic features. Epilepsy Behav. http://dx.doi.org/10.1016/j.yebeh.2015.06.014.
Yang, M., Bozdagi, O., Scattoni, M.L., Wohr, M., Roullet, F.I., Katz, a.M., Abrams, D.N., Kalikhman, D., Simon, H., Woldeyohannes, L., Zhang, J.Y., Harris, M.J., Saxena, R., Silverman, J.L., Buxbaum, J.D., Crawley, J.N., 2012. Reduced Excitatory Neurotransmission and Mild Autism-Relevant Phenotypes in Adolescent Shank3 Null Mutant Mice. J. Neurosci. 32:6525–6541. http://dx.doi.org/10.1523/JNEUROSCI.6107-11.2012.
Zeilhofer, H.U., Wildner, H., Yevenes, G.E., 2012. Fast synaptic inhibition in spinal sensory processing and pain control. Physiol. Rev. 92:193–235. http://dx.doi.org/10.1152/physrev.00043.2010.